Journal of Marine Systems, 1 (1990) 119–154
Elsevier Science Publishers B.V., Amsterdam – Printed in The Netherlands

Sensitivity of wind-driven tropical Pacific Ocean simulations on seasonal and interannual time scales

A.J. Busalacchi [1], M.J. Mcphaden [2], J. Picaut [3] and S.R. Springer [4]

[1] *Laboratory for Oceans, NASA / Goddard Space Flight Center, Greenbelt, MD (U.S.A.)*
[2] *NOAA Pacific Marine Environmental Laboratory, Seattle, WA (U.S.A.)*
[3] *Groupe SURTROPAC, Institut Français de Recherche Scientifique pour le Développement en Coopération (ORSTOM), Nouméa, New Caledonia*
[4] *School of Oceanography, University of Washington, Seattle, WA (U.S.A.)*

Received November 17, 1989; revised version accepted November 27, 1989

ABSTRACT

Busalacchi, A.J., McPhaden, M.J., Picaut, J. and Springer, S.R., 1990. Sensitivity of wind-driven tropical Pacific Ocean simulations on seasonal and interannual time scales. J. Mar. Syst., 1: 119–154.

The purposes of this study are (1) to characterize differences in the time/space structure of various multiyear surface wind products for the tropical Pacific; and (2) to quantify the impact these differences may have on our ability to model oceanic wind-forced variability on seasonal and interannual time scales. Three coincident wind field analyses are used, viz. the Florida State University (FSU) subjective analysis, the University of Hawaii (SAWIN) subjective analysis and the Fleet Numerical Oceanography Center (FNOC) operational analysis. The five years chosen for study, 1979–1983, encompass three years of a fairly regular seasonal cycle leading up to the 1982–1983 El Niño. A linear multi-vertical model model is forced with these analyses; model dynamic height and sea level are then compared with observations based on expendable bathythermograph and island tide gauge data. The mean seasonal cycle prior to El Niño (1979–1981) is considered first, which then serves as a self-consistent basis for analyzing the interannual variability, particularly the significant anomalies about the mean in 1982–1983.

The impact of discrepancies in the forcing functions is discussed relative to the dominant seasonal and interannual scales of variability for the wind-driven oceanic response. The analyses of the wind products and model solutions indicate the need for special attention to the wind stress curl fields when evaluating wind products for use in tropical oceanographic applications. On seasonal time scales, critical differences in the wind stress products, of order 0.2–0.4 dyn cm^{-2}, are in wind regimes of surface convergence and significant gradients such as the ITCZ and SPCZ. These uncertainties in the wind fields, or more appropriately the wind stress curl distributions, are manifested in model sea level solutions as 6–12 cm discrepancies near the NECC Trough and east of New Guinea. On average, the seasonal amplitude of the wind-forced sea level response in any one simulation is of the same order as the differences between any two sea level simulations.

The interannual variability is dominated by the anomalies associated with the 1982–1983 El Niño. Root mean square differences between the product versus product wind stress anomalies range from 0.1–0.2 dyn cm^{-2} along the major ship tracks and up to 0.5 dyn cm^{-2} away from the shipping lanes. The basin-wide average of the rms differences, approximately 0.25 dyn cm^{-2}, is of similar magnitude to the average wind stress anomaly. Discrepancies in the interannual variability of the wind products lead to large-scale differences in the model sea level anomalies of up to 9–21 cm. The anomalous year to year variability of model sea level is of similar order in each of the simulations. Results for the FSU and SAWIN forced simulations are generally in better agreement with the observations than the FNOC simulation, especially during the 1982–1983 El Niño.

0924-7963/90/$03.50

Introduction

The importance of the role of the tropical oceans in global change is undenied. Over the past fifteen years our empirical understanding of tropical ocean circulation has benefited greatly from many field programs (e.g. INDEX, NORPAX, PEQUOD, EPOCS, SEQUAL/FOCAL, TROPIC HEAT and WEPOCS). In parallel with these observational studies, our theoretical approach has advanced from analytical and reduced-gravity models driven by idealized forcing functions, through ocean general circulation model simulations driven by observed winds, to coupled atmosphere–ocean model studies. One basic underpinning common to these studies is that, to first order, the tropical ocean response to atmospheric forcing is deterministic on time scales from months to years (WCRP, 1985). This is in stark contrast to the stochastic variability indicative of mid-latitude ocean circulation. Given accurate initial conditions and surface atmospheric forcing, the deterministic prediction of tropical ocean circulation may be possible. It was this prospect for the prediction of tropical ocean variability that led, in part, to the formation of the Tropical Ocean Global Atmosphere (TOGA) Program.

At the present time however, we do not possess sufficiently accurate forcing functions. Previous ocean modelling studies have concluded that any improvement in our ability to model the upper tropical ocean circulation must start with an improvement in our ability to describe the state of the surface wind field. For example, tropical Pacific model simulations have demonstrated that the quality of sea level hindcasts is higher along the equator and eastern boundary where the response is an integral function of the equatorial zonal wind stress to the west (Busalacchi and Cane, 1985). The quality of sea level hindcasts is degraded away from the equator where a portion of the solution is determined by a derivative of the forcing, i.e., the wind stress curl. Random errors present in wind stress data tend to have a greater influence off the equator where they are differentiated, as opposed to on the equator where their effect is integrated.

In 1985, at the beginning of the ten-year TOGA Program, the required accuracy and resolution for surface wind stress were 0.1 dynes cm^{-2} on a monthly mean basis over spatial scales of 2° latitude by 10° longitude (WCRP, 1985). During the first half of the TOGA Program there has been little progress in meeting these requirements. As a result of the logistical problems in monitoring the surface wind field over all tropical oceans, it is difficult to assess quantitatively the accuracy of gridded fields of surface wind stress generated presently from sparse ship, buoy, island and cloud motion observations or from operational center analyses. Little is known even of the similarities or differences, on both seasonal and interannual time scales, among the various wind products available today.

The next five years of TOGA may see the launch of two satellite scatterometers (ERS-1, 1990; NSCAT, 1995) and the implementation of a wind recorder array within ±8° of the equator across the tropical Pacific (Hayes, 1989). However, until the time that these projects are operational and prove successful in meeting the accuracy and coverage requirements for TOGA wind measurements, there remains a need to quantify the seasonal and interannual discrepancies in wind data presently available as forcing functions for tropical ocean models. Moreover, assessment of the impact of these uncertainties on our ability to model the tropical ocean circulation is essential.

The present study has been designed to begin to address these shortcomings in our knowledge of the limitations in surface wind data and subsequent effect on tropical ocean simulations. First, the various wind products available for tropical ocean circulation studies will be intercompared on seasonal and interannual time scales. Subsequently, those same data will be used in a series of tropical ocean model simulations. We seek to determine how much error in the simplest of wind-driven ocean simulations can be attributed to errors in the description of the wind field.

The surface wind field is also an important factor in the determination of sensible and latent heat fluxes and so an ocean general circulation model would be the appropriate model of choice for investigating the fully nonlinear, dynamic and thermodynamic response to surface wind forcing

(cf. Harrison et al., 1989). In the present study we want to keep the assessment of the impact of limitations in surface wind data as straightforward as possible. The most direct way of doing so is to consider the dynamic, wind-driven response via vertically integrated variables such as sea level, dynamic height and heat content that tend to average out nonlinear, nonadiabatic effects. A linear ocean model, when viewed as a transfer function for surface wind stress data, is the most efficient way of assessing the impact of uncertainties in such data on the dynamic oceanic response. The efficiency in this approach also allows multiyear simulations to be considered. Thus the effects of uncertainties in the normal or mean seasonal wind forcing can be contrasted with those for the interannual variability (e.g. those wind anomalies representative of El Niño events).

We have chosen to illustrate the sensitivity of tropical ocean models to wind forcing by investigating variations in the Pacific for the years 1979 through 1983. This permits the fairly regular seasonal cycle present in 1979–1981 to be contrasted with the 1982–1983 El Niño often referred to as the event of the century (Enfield, 1989). For these five years there are three different wind data sets available, each of which was the result of a consistent analysis scheme for the entire period. We will consider the seasonal and interannual signals among the wind products and then the differences. Next, the impact of the signals and differences in the wind products will be assessed by considering the similarities and differences in wind-driven seasonal and interannual model sea level solutions.

The implications of uncertainties in the wind field will be illustrated by intercomparing the model sea level solutions with contemporaneous in situ data such as expendable bathythermograph (XBT) derived dynamic heights and tide gauge sea level observations. The results will show those regions with the greatest uncertainty in the modelled wind-driven response. Analyses of the wind data, together with the model solutions, will also show those regions where additional measurements and improvements in wind field estimates are needed.

The wind stress data and the ocean model used are described in the next section. The annual mean and seasonal variabilities for the wind stress data and model sea level solutions are presented in the third section. The interannual variability, depicted as anomalies about the mean seasonal cycle, follows in the fourth section. Intercomparisons between the model sea level and in situ data are discussed in the fifth section. Major conclusions are summarized and discussed in the last section.

Wind stress products and ocean model

(a) Wind data

The period of interest, 1979–1983, was chosen because it provided an interesting contrast between a fairly regular mean seasonal cycle for 1979–1981 and the extreme El Niño event that followed in 1982–1983. More importantly, this five-year period was chosen because more than one wind product was available. For these particular years of study there are three different wind stress products available, each resulting from a consistent analysis scheme over the full five years. Two of these data sets are derived from subjective analyses and the third is derived from an operational objective analysis. A constant drag coefficient of 1.5×10^{-3} is used to convert from wind to wind stress for each of the three wind data sets.

One of the subjective analyses is the Florida State University (FSU) analysis of ship-board observations provided by J.J. O'Brien. The analysis procedure of transforming individual ship wind observations into monthly mean wind stress fields on a $2° \times 2°$ grid is described by Goldenberg and O'Brien (1981). The second subjective analysis is a combination of satellite-observed, low-level cloud motion vectors (east of the dateline), ship wind observations, island wind observations and buoy wind observations performed by J. Sadler at the University of Hawaii. The production of monthly mean surface wind and wind stress data sets on a $2.5° \times 2.5°$ grid is described by Sadler and Kilonsky (1985) and Sadler et al. (1987). These data, based in part on satellite-derived cloud track winds, will be referred to as SAWIN. The third data set is an objectively analyzed operational

product from the Global Band Analyses of the U.S. Navy's Fleet Numerical Oceanography Center (FNOC). An objective analysis based on Cressman (1959) is used on all reports (ship, island, buoy, etc.) in an operational data base for 6-hour intervals on a $2.5° \times 2.5°$ grid. Six-hourly stresses are computed and averaged to form monthly means. We chose not to use wind products from other operational centers such as the National Meteorological Center (NMC) and the European Center for Medium Range Weather Forecasts (ECMWF) because their analysis schemes were changed within the five years of this study (Bengtsson and Shukla, 1989). The use of continuous multiyear time series of data from operational centers in research studies is often difficult because the operational centers periodically update and improve their methodology to meet their operational objective of providing the best possible analysis-forecast product.

(b) Ocean model

A linear, numerical treatment of the shallow water wave equations is used as a transfer function to analyze the wind-driven dynamic response of a model tropical Pacific Ocean to different representations of the surface wind stress. The model basin extends from 20°N to 20°S and 126°E to 70°W. The open boundary condition of Roed and Smedstad (1984) is applied to the northern and southern boundaries and a no-slip condition is imposed along the idealized coastal boundaries. The horizontal resolution of the model is 40 km between the same variables. For the purposes here, sea level is the variable of interest. Model height field solutions, in response to the monthly mean wind forcing, are generated for the first four baroclinic modes of a Brunt–Vaisala frequency profile based on CTD data between $\pm 1.5°$ of the equator at 179°W (Eriksen et al., 1983). A final sea level solution is found by summing the individual contributions to sea level from each of the four vertical modes. A more complete description of the model is provided in McPhaden et al. (1988a), who used this model to simulate the mean seasonal response of tropical Pacific sea level and dynamic height. A similar model was also used by Busalacchi and Cane (1985) in hindcasting the sea level onset of the 1982–1983 El Niño.

Here we consider both the mean seasonal cycle during the pre-El Niño period 1979–1981 and the interannual anomalies for 1979–1983. The model was spun up from rest using the mean seasonal wind stress from 1979–1981. After an exact repeating seasonal cycle was obtained (i.e. all initial transients had died out), a five-year integration was forced by the individual monthly mean wind stresses for January 1979 through December 1983. The mean seasonal cycle of sea level was formed from the first three years of integration 1979–1981. In view of the linear dynamics, this is equivalent to the seasonal equilibrium obtained after spin-up in response to the mean seasonal wind stress for 1979–1981. Examination of the interannual variability is based on the anomalies formed by subtracting the mean seasonal cycle (1979–1981) from the five-year time series (1979–1983).

Analyses of the wind stress products and model sea level responses proceed in parallel. Intercomparisons of the winds are based on the fields of the zonal wind stress τ^x, meridional wind stress τ^y and the wind stress curl $\nabla x \vec{\tau}$. These three fields were singled out since they represent the dominant forcing of the local sea level response for the equator, side boundaries and interior, respectively. The signal for each wind stress field and model sea level solution is characterized by an annual mean, a standard deviation of the mean seasonal cycle 1979–1981 and a standard deviation for the interannual anomalies 1979–1983. Root mean square differences between the wind stress products and among the wind-forced sea level solutions are presented for both the mean seasonal cycle and the interannual anomalies. These RMS differences are viewed as representing a lower bound to the uncertainty or noise within this set of wind products and model sea level solutions. Approximate signal to noise ratios are obtained by forming standard deviation/RMS difference ratios for the seasonal and interannual variabilities of the wind stress and sea level.

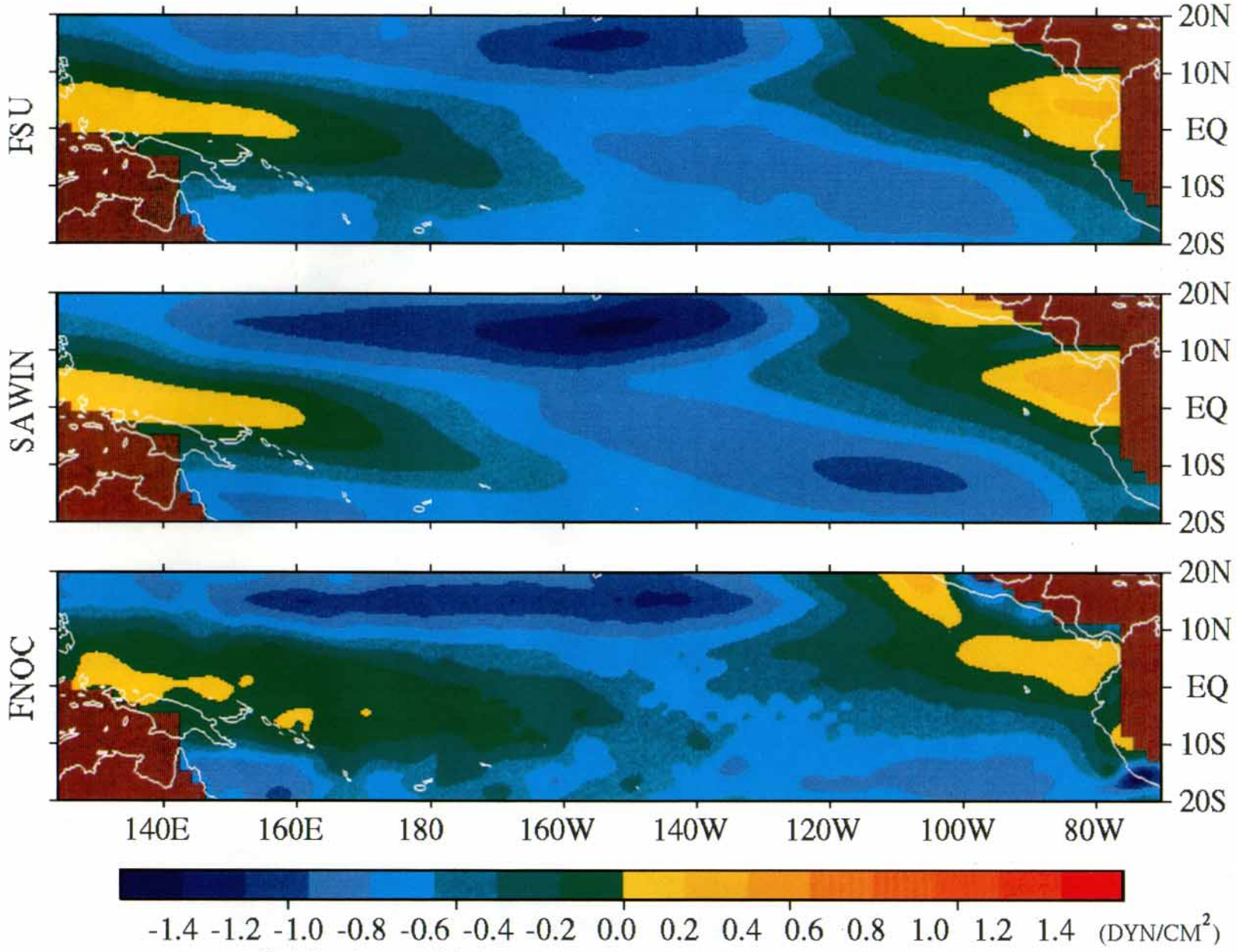

Fig. 1. Annual mean zonal wind stress, τ^x, 1979–1981: (Top) FSU (Middle) SAWIN (Bottom) FNOC

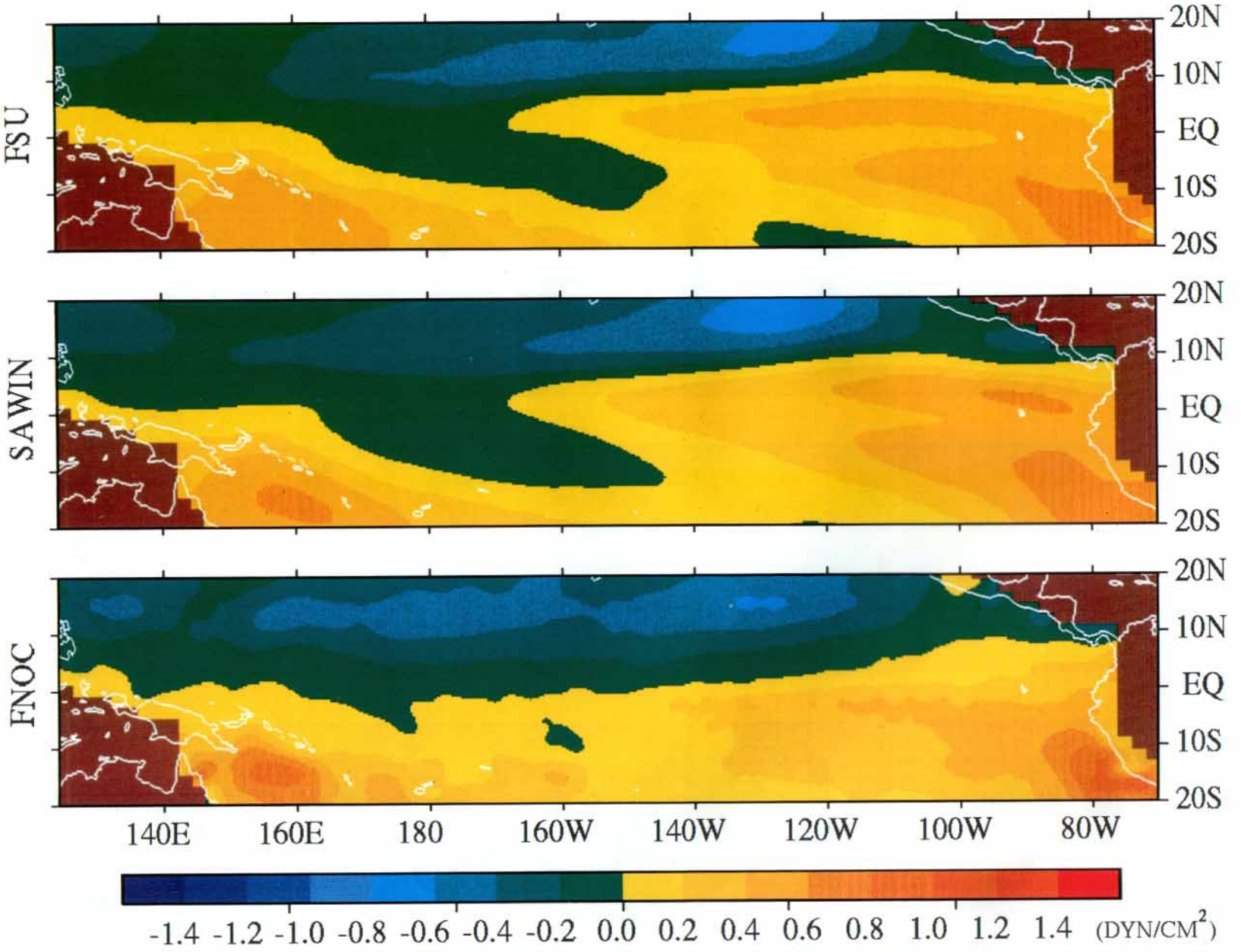

Fig. 2. Annual mean meridional wind stress, τ^y, 1979–1981: (Top) FSU (Middle) SAWIN (Bottom) FNOC

Mean seasonal forcing and model sea level response

(a) Annual mean

(i) Wind stress

The annual mean zonal and meridional wind stresses for the pre-El Niño years of 1979–1981 are presented in Fig. 1 and 2. Several large-scale features of the wind field are common to all three wind stress products. The central and eastern portions of the basin are dominated by the core regions of the northeast and southeast trade winds separated by the Inter-Tropical Convergence Zone (ITCZ). In the west, the South Pacific Convergence Zone (SPCZ) separates southeasterlies to the south from more zonal winds to the north. Weak westerlies along the equator on both ends of the basin are present in all three data sets. Among the three wind products, these large-scale patterns appear to be the most similar within the FSU and SAWIN data.

With respect to differences among the data, the SAWIN wind stress, in general, has the strongest mean fields. These data are characterized by larger zonal length scales, and reflect an explicit zonal smoothing applied to the observations during the subjective analysis (J. Sadler, pers. commun., 1987). In contrast, the FNOC data contains the most small-scale structure. The easterly component to the southeast trades is noticeably weaker in the FNOC wind stress. An important qualitative difference in the meridional wind stress fields is the mean position of the ITCZ. Assuming the line of zero meridional wind stress is representative of the mean position of the ITCZ (Fig. 2), we note that the ITCZ is considerably further south in the FNOC data. These FNOC meridional wind stresses are also more antisymmetric about the equator since there is no mean extension of northerlies into the southern hemisphere near the dateline. Near the coasts in the southern hemisphere, the FNOC southerly wind stress is significantly stronger than either the FSU or SAWIN wind stresses.

Several of the attributes of the individual wind stress components are accentuated when these fields are differentiated to form the annual mean wind stress curl (Fig. 3). The large-scale structure in all three products is characterized by alternating bands of positive and negative wind stress curl. Once again, the FSU and SAWIN products are most similar, with the SAWIN wind stress curl being the smoothest and having the larger zonal length scales. The small-scale structure evident in the FNOC τ^x and τ^y components is magnified in the curl field, both in the interior and near the coasts. One particularly important difference in the wind stress curl distributions is in the southern hemisphere. South of the equator in the FSU and SAWIN data, two regions of negative curl (cyclonic) are separated by an area of positive curl (anticyclonic). In the FNOC data, however, the cyclonic curl extends all the way across the southern part of the basin.

(ii) Model sea level response

The annual mean sea level in response to the mean wind stress forcing is depicted in Fig. 4. The model sea level topography is characterized by alternating troughs and ridges which delineate the major zonal surface current systems. For example, a well defined North Equatorial Countercurrent (NECC) trough is common to all three sea level solutions near 10° N. This feature is a direct result of the continuous band of cyclonic wind stress curl common to all three wind products. Since the mean wind stress curl distributions for FSU and SAWIN are similar, so are the corresponding mean sea levels. The most striking difference is with the FNOC solution where an annual mean South Equatorial Countercurrent (SECC) trough extends all the way across the basin in the southern hemisphere. This feature, that has no counterpart in either the FSU or SAWIN forced sea level solutions, is caused by the continuous band of cyclonic wind stress curl that is present in the FNOC data south of the equator (Fig. 3). The presence of this SECC trough in the FNOC simulation results in a symmetric meridional topography that is not found in the FSU or SAWIN-forced sea level topographies. The smaller-scale structure that was noted in FNOC wind stress curl field has little effect in this Sverdrup-like response in the interior (cf. Landsteiner et al., 1990).

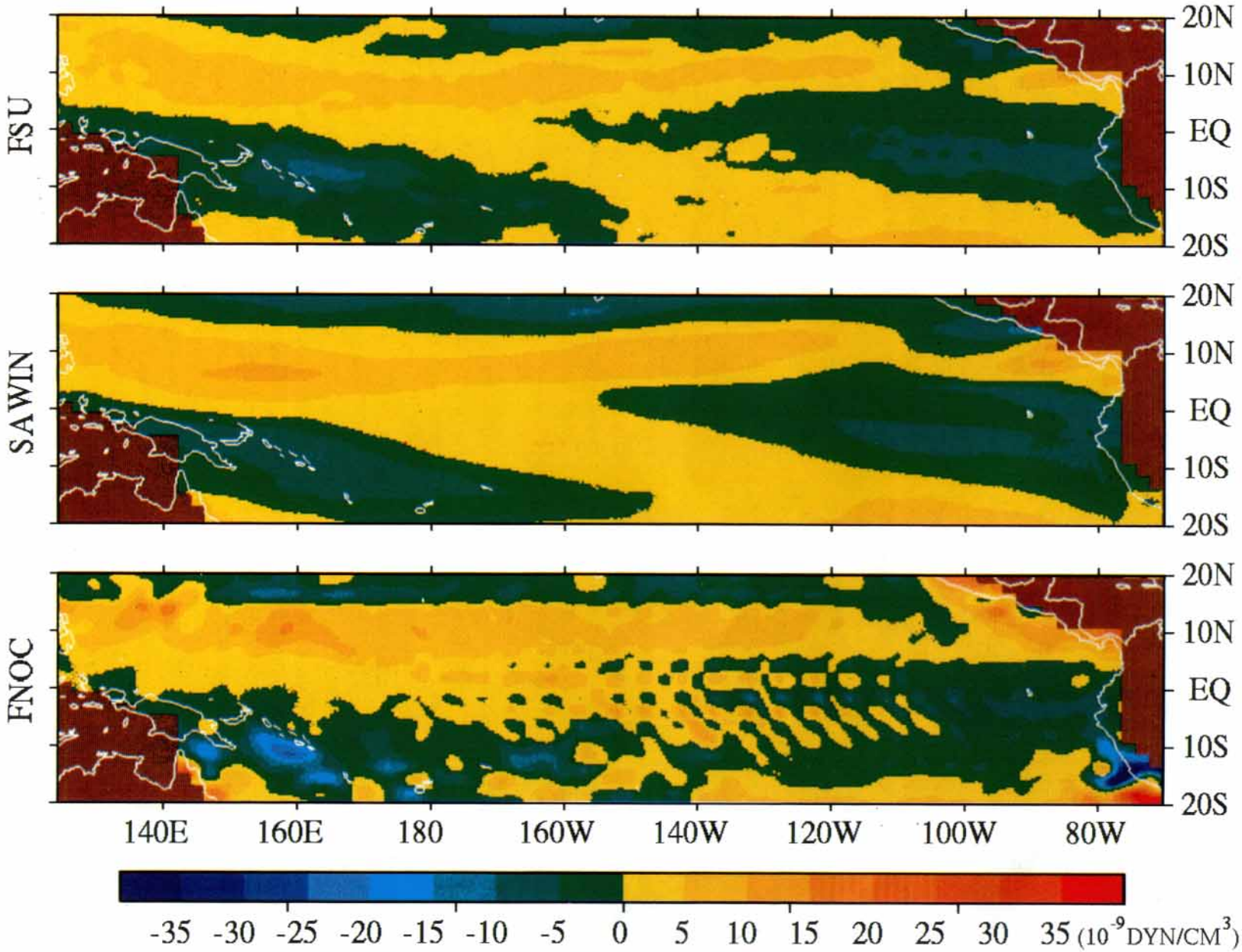

Fig. 3. Annual mean wind stress curl, $\nabla \times \vec{\tau}$, 1979–1981: (Top) FSU (Middle) SAWIN (Bottom) FNOC

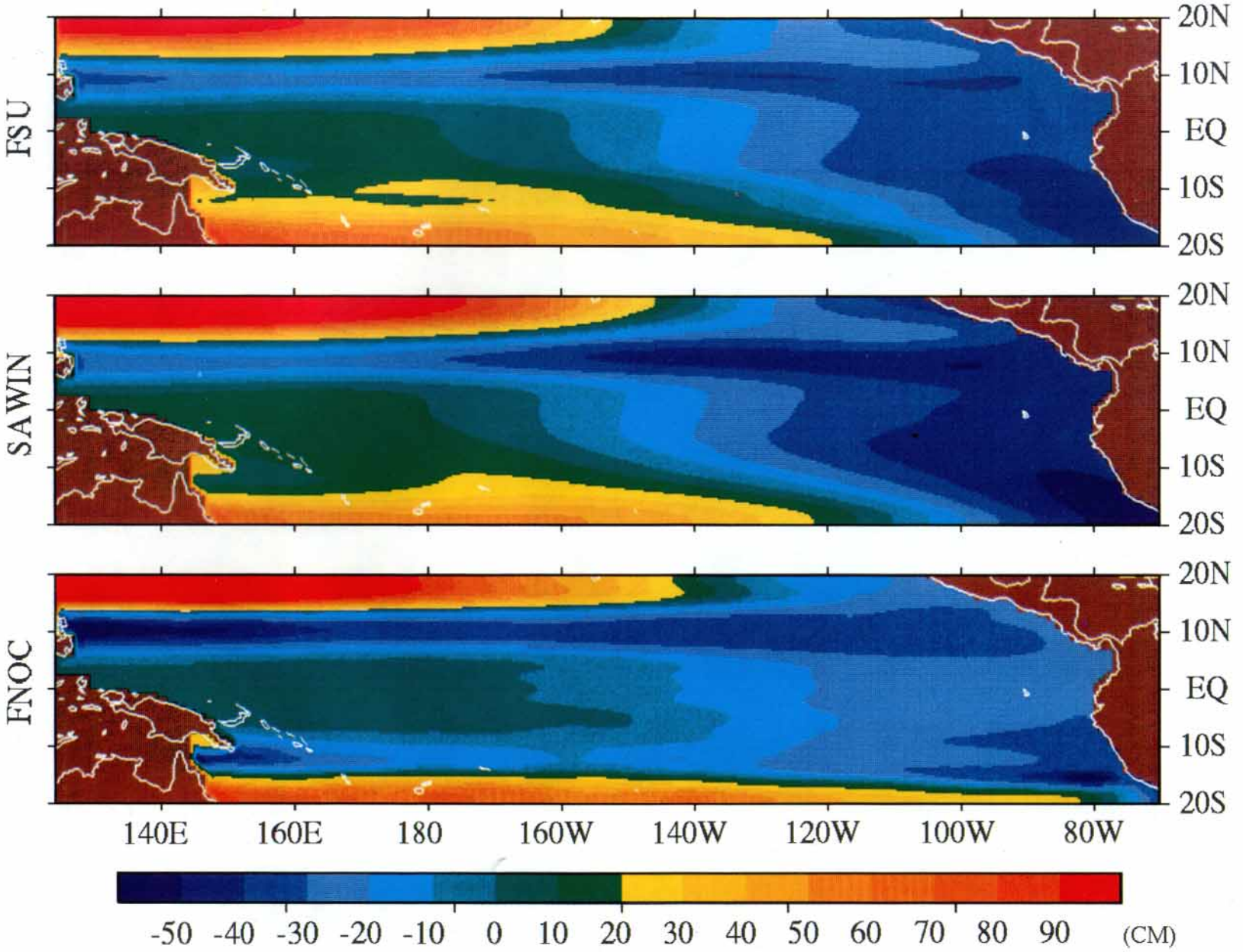

Fig. 4. Annual mean model sea level topography, 1979–1981, in response to forcing by: (Top) FSU wind stress (Middle) SAWIN wind stress (Bottom) FNOC wind stress

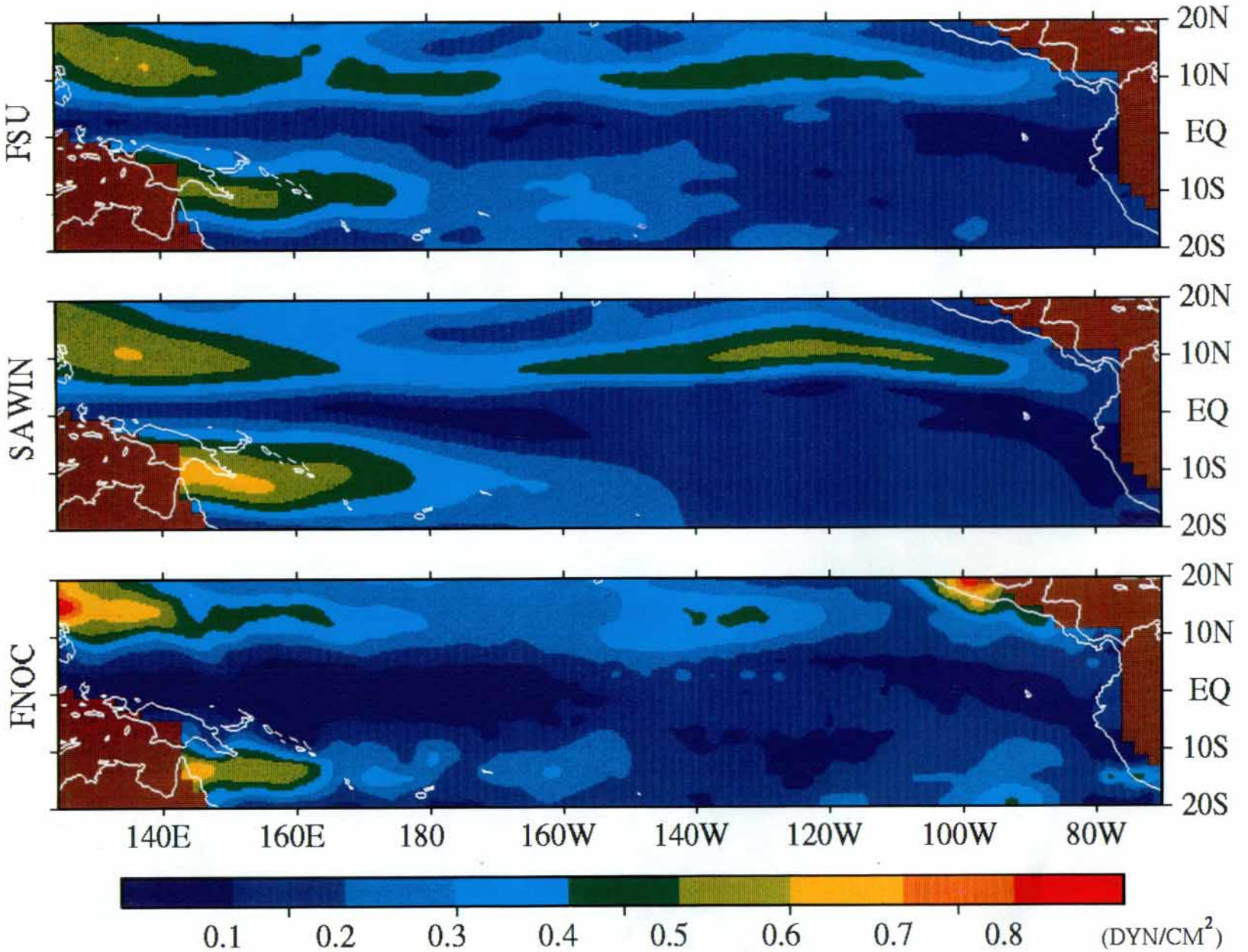

Fig. 5. Standard deviation of the mean seasonal cycle (1979–1981) of τ^x: (Top) FSU (Middle) SAWIN (Bottom) FNOC

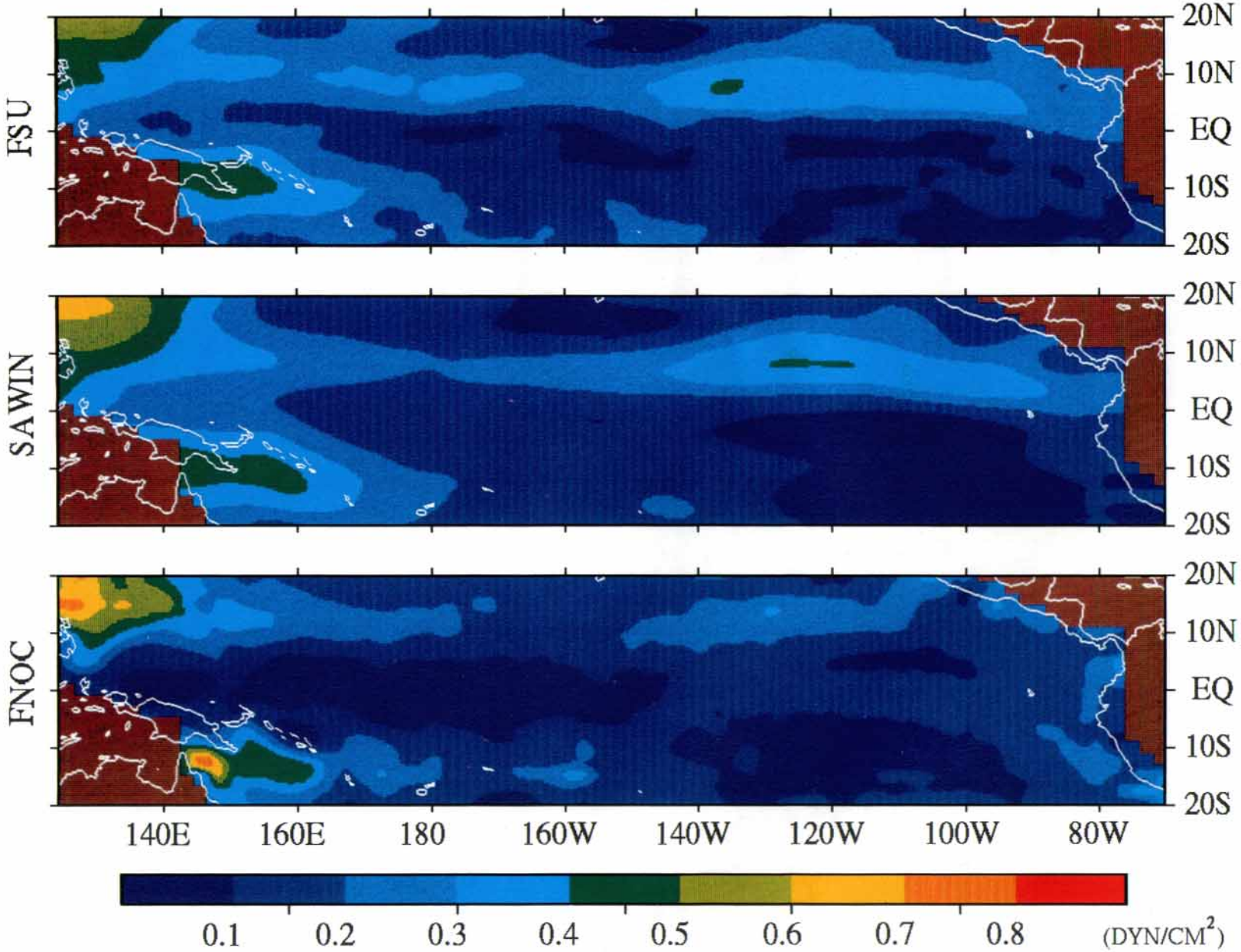

Fig. 6. Standard deviation of the mean seasonal cycle (1979–1981) of τ^y: (Top) FSU (Middle) SAWIN (Bottom) FNOC

(b) Seasonal variations

(i) Wind stress

The seasonal fluctuations of the wind stress components are quantified in terms of the standard deviation of the mean seasonal cycle σ_s, for 1979–1981 (Figs. 5, 6). The dominant large-scale seasonal changes, $\sigma_s \sim 0.4$–0.7 dyn cm^{-2}, are associated with the seasonal excursions of the ITCZ in the northern hemisphere and the monsoon circulation of both hemispheres in the west. Basin wide, the annual harmonic is responsible for 60–80% of the variance in the mean seasonal cycle. As was the case for the mean fields, the FSU and SAWIN data have similar seasonal structure, with the maxima of the SAWIN data being slightly larger in amplitude and having elongated zonal scales. The seasonal amplitude of the northeast trades is much weaker in the FNOC wind stress. The largest seasonal changes in any of the wind stress products, $\sigma_s > 0.7$ dyn cm^{-2}, are situated near the coasts in the FNOC data. Areal averages of these fields from 20°N to 20°S are compiled in Table 1.

When viewed in terms of the wind stress curl (Fig. 7), the largest seasonal changes are clearly defined and zonally oriented in the SAWIN data, straddling the mean position of the ITCZ, $\sigma_s > 6 \times 10^{-9}$ dyn cm^{-3}. This data set also depicts a broad region of low wind stress curl variability, $\sigma_s < 2 \times 10^{-9}$ dyn cm^{-3}, in the southeastern portion of the basin. Seasonal variability in the FSU wind stress curl exhibits some aspects of the same large-scale structure, but the amplitude maxima are smaller and obscured by small-scale fluctuations. The seasonal variability of the FNOC wind stress curl has no larger-scale structure in the interior, but rather is dominated by very large changes, $\sigma_s > 18 \times 10^{-9}$ dyn cm^{-3}, near the extreme ends of the basin.

TABLE 1

Mean seasonal cycle 1979–1981

Areally Averaged Standard Deviation ($\overline{\sigma_s}$)	τ^x (dyn cm^{-2})	τ^y (dyn cm^{-2})	$\nabla x \vec{\tau}$ (10^{-9} dyn cm^{-3})	sea level (cm)
FSU	0.25	0.20	5.08	3.76
SAWIN	0.25	0.20	4.31	3.76
FNOC	0.20	0.16	4.28	3.11
Root Mean Square Difference ($\overline{\text{RMSD}}$)				
FSU-SAWIN	0.14	0.09	4.08	3.16
FSU-FNOC	0.17	0.14	5.46	3.51
SAWIN-FNOC	0.15	0.11	4.71	3.57

Quantitative differences in the mean seasonal variability of the wind stress products are described in terms of the root mean square difference (RMSD) between the seasonal cycles (less the means) of the three possible product pairs (Figs. 8, 9). Generally, the largest RMS differences, RMSD ~ 0.2–0.4 dyn cm^{-2}, are situated near 8–10°N and in the southern hemisphere where there are few wind observations. The largest RMS differences are often coincident with the largest seasonal fluctuations, i.e., where the signal is largest so is the uncertainty. The RMS difference between the two subjective analyses (FSU and SAWIN) is the smallest, RMSD < 0.24 dyn cm^{-2}. Accordingly, RMS differences with the operational FNOC data are the largest, especially in the vicinity of the ITCZ and SPCZ, RMSD > 0.24 dyn cm^{-2}.

These discrepancies in the seasonal cycles of τ^x and τ^y for the three products are significantly less than the seasonal signals represented by σ_s for any one product. The basin-wide mean $\overline{\text{RMS}}$ differences for the three product combinations are quite similar, approximately 0.15 dyn cm^{-2} for τ^x and 0.11 dyn cm^{-2} for τ^y (Table 1). If these mean discrepancies are taken to represent a measure of the uncertainty or noise, and subsequently used to normalize the mean seasonal signals $\overline{\sigma_s}$ of Table 1, approximate signal to noise ratios ($\overline{\sigma_s}/\overline{\text{RMSD}}$) of 1.1 to 2.2 are obtained.

There are no systematic differences in the seasonal variability of the wind stress curls (Fig. 10). The range of the RMS differences on the basin scale is 4–8×10^{-9} dyn cm^{-3}. Localized maxima of 8–16×10^{-9} dyn cm^{-3} are present near the coasts in the rms differences with the FNOC seasonal wind stress curl. The signal/noise ratios for the seasonal variability of the wind stress curl range between 0.8–1.2. It is worth noting that these ratios for the wind stress curl are less than those obtained for the individual wind stress curl

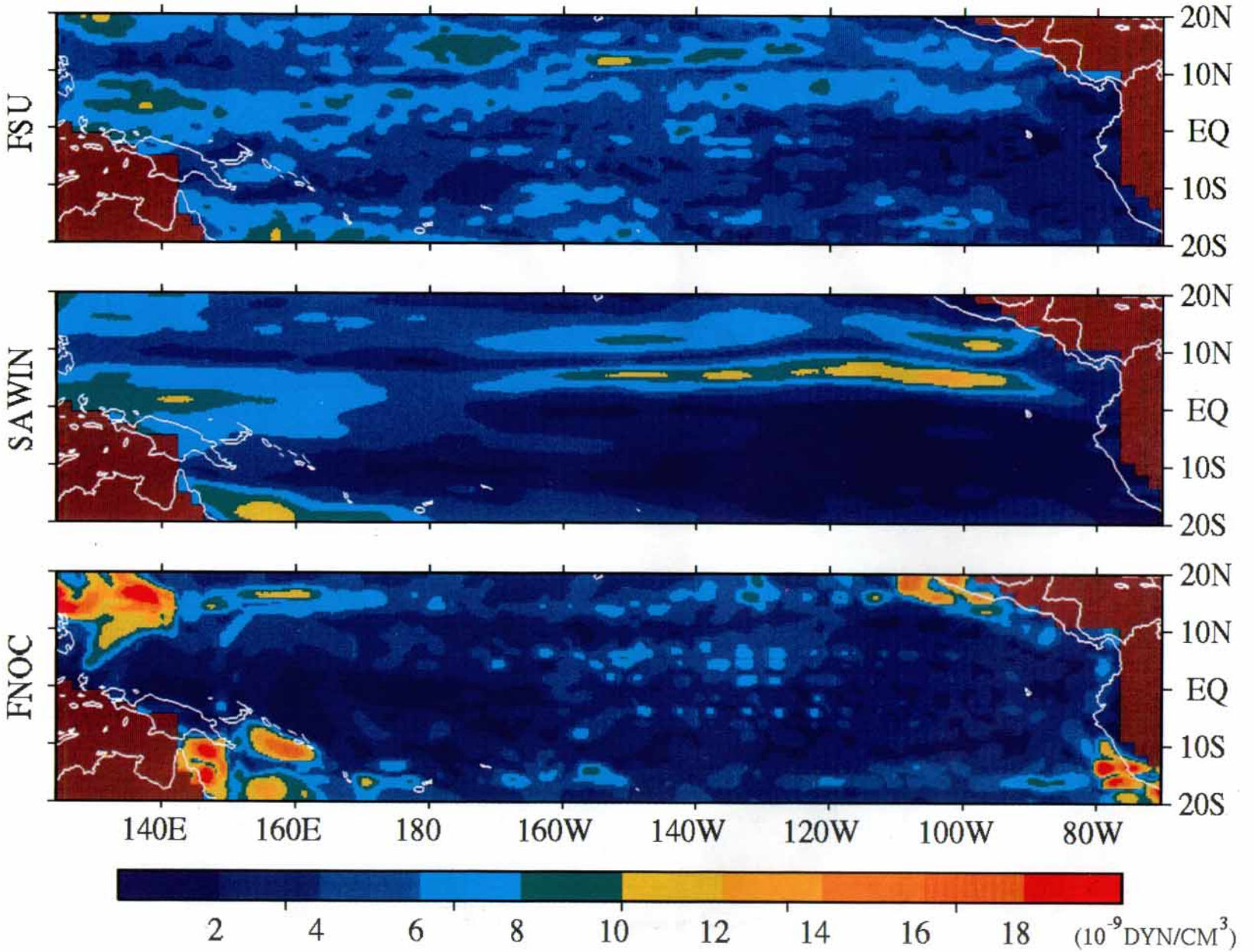

Fig. 7. Standard deviation of the mean seasonal cycle (1979–1981) of $\nabla x \vec{\tau}$: (Top) FSU (Middle) SAWIN (Bottom) FNOC

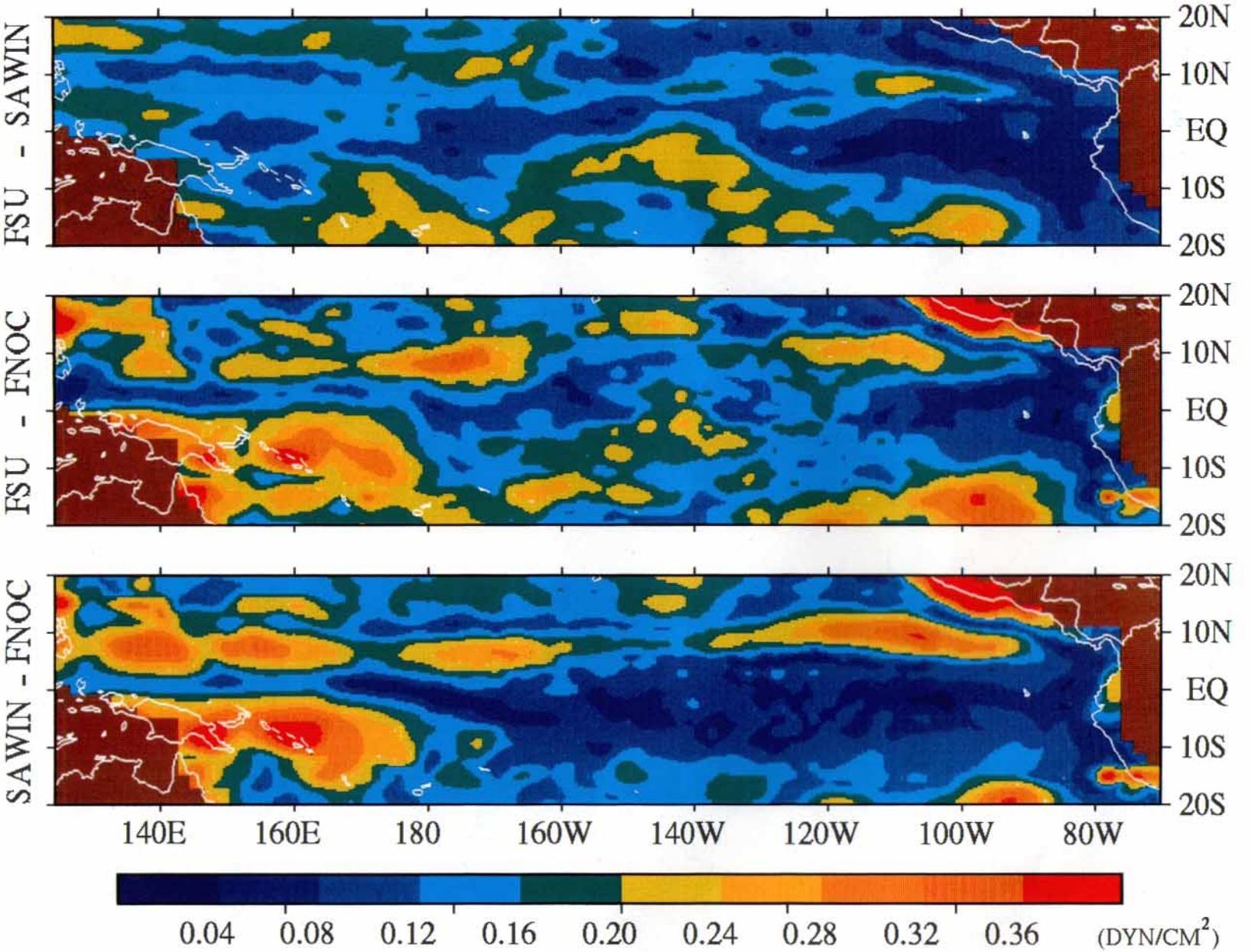

Fig. 8. Root mean square difference between the mean seasonal cycles of τ^x for: (Top) FSU-SAWIN (Middle) FSU-FNOC (Bottom) SAWIN-FNOC

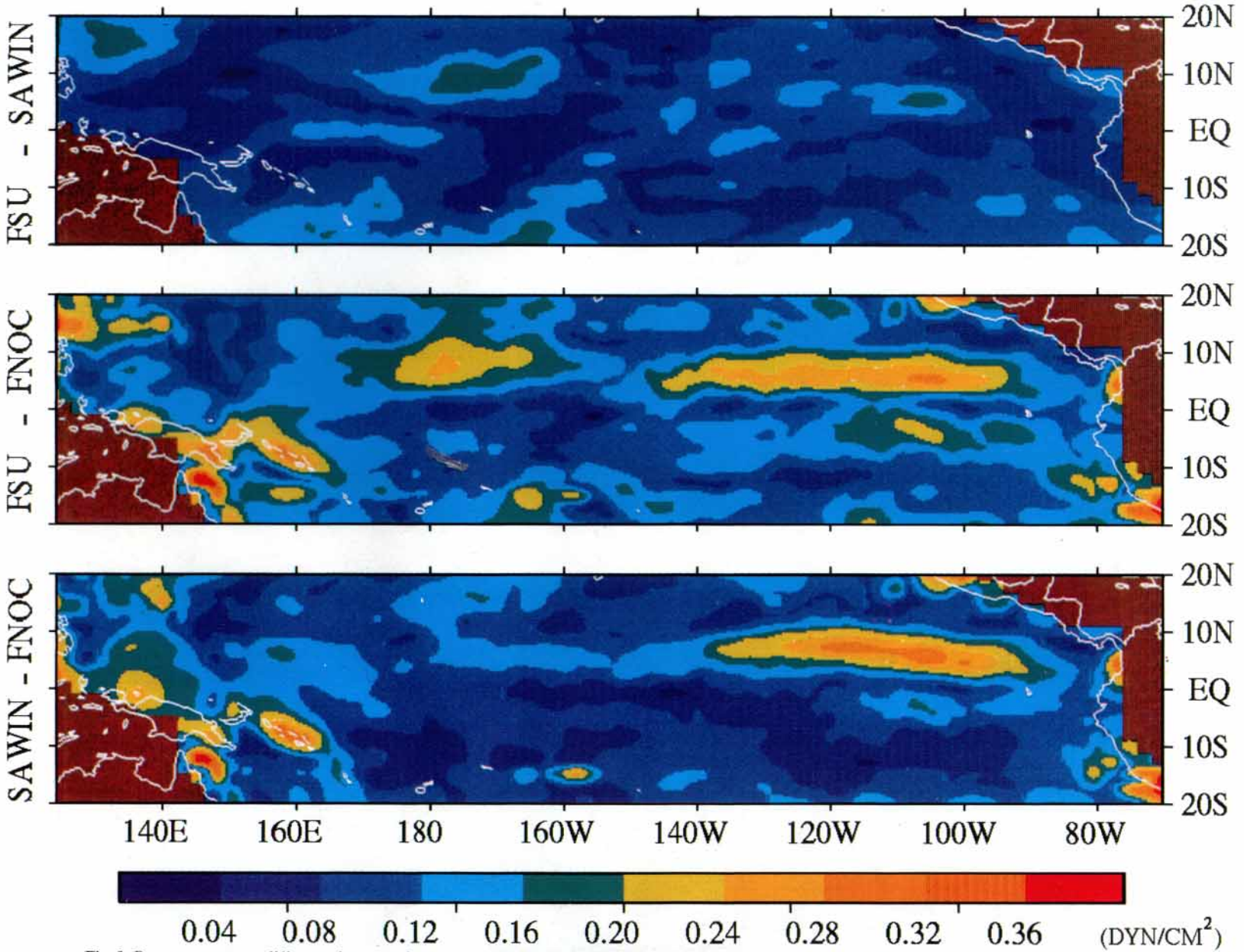

Fig. 9. Root mean square difference between the mean seasonal cycles of τ^y for: (Top) FSU-SAWIN (Middle) FSU-FNOC (Bottom) SAWIN-FNOC

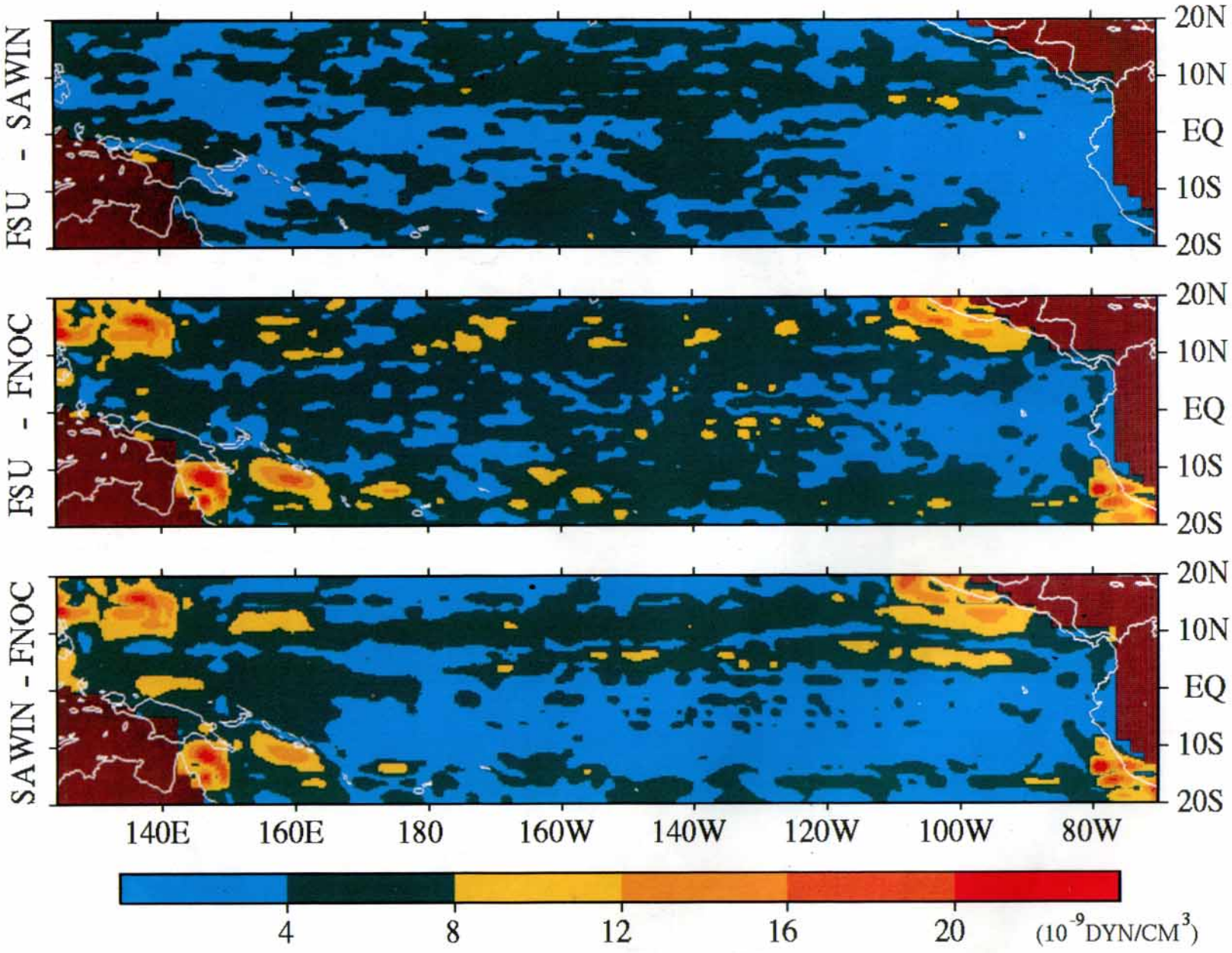

Fig. 10. Root mean square difference between the mean seasonal cycles of $\nabla x\vec{\tau}$ for: (Top) FSU-SAWIN (Middle) FSU-FNOC (Bottom) SAWIN-FNOC

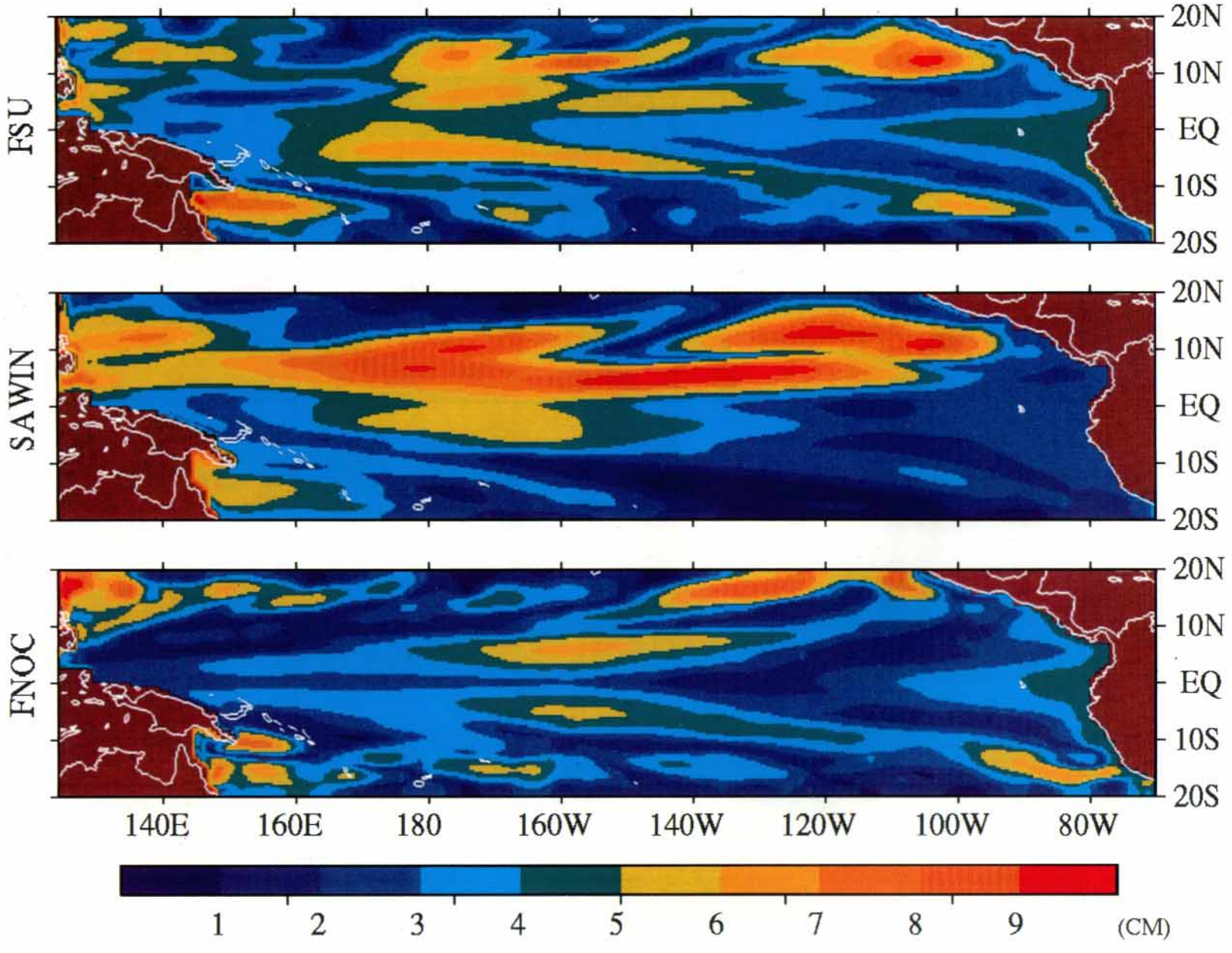

Fig. 11. Standard deviation of the mean seasonal cycle (1979–1981) of model sea level in response to forcing by: (Top) FSU wind stress (Middle) SAWIN wind stress (Bottom) FNOC wind stress

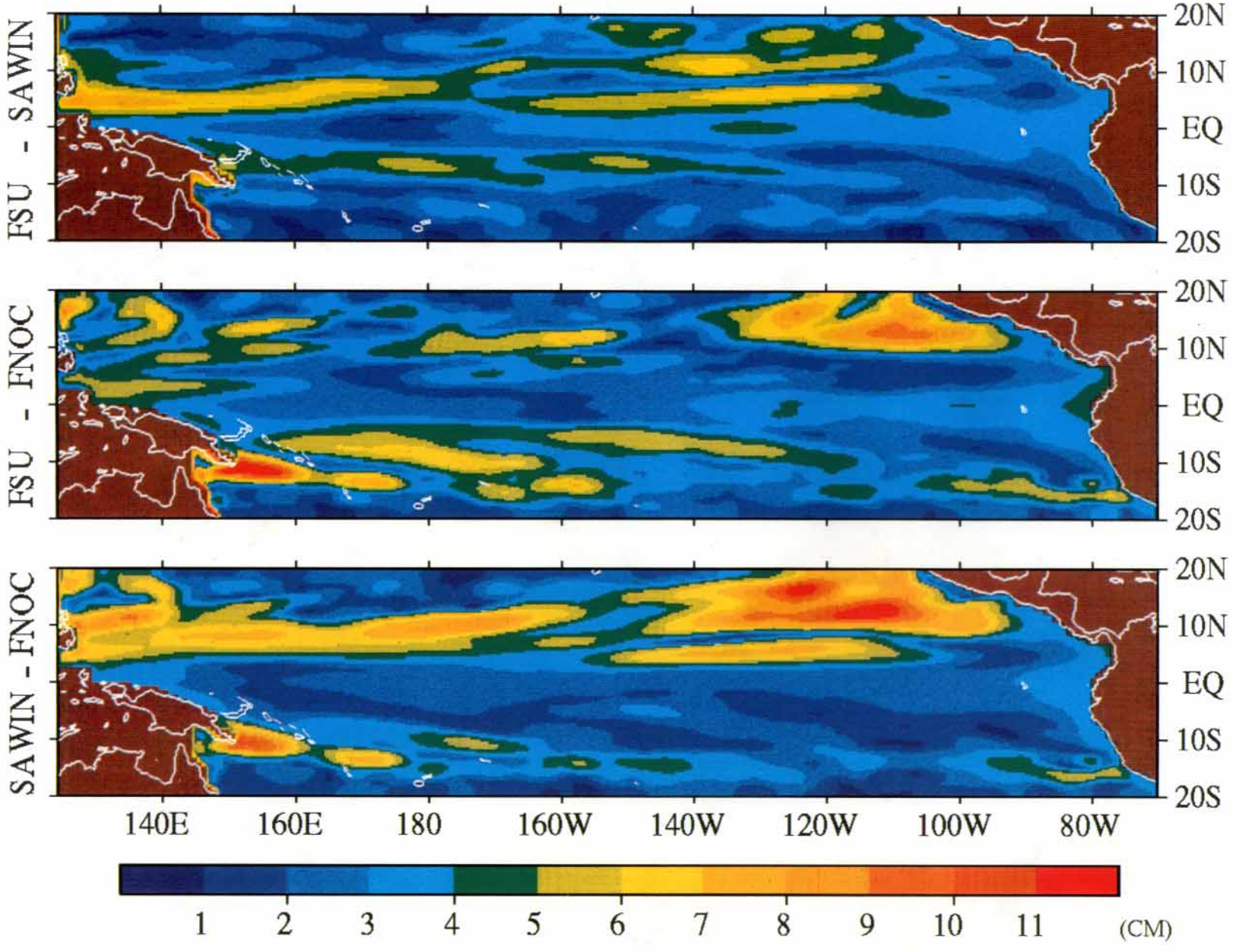

Fig. 12. Root mean square difference between the mean seasonal cycles of model sea level in response to forcing by the two wind products: (Top) FSU-SAWIN (Middle) FSU-FNOC (Bottom) SAWIN-FNOC

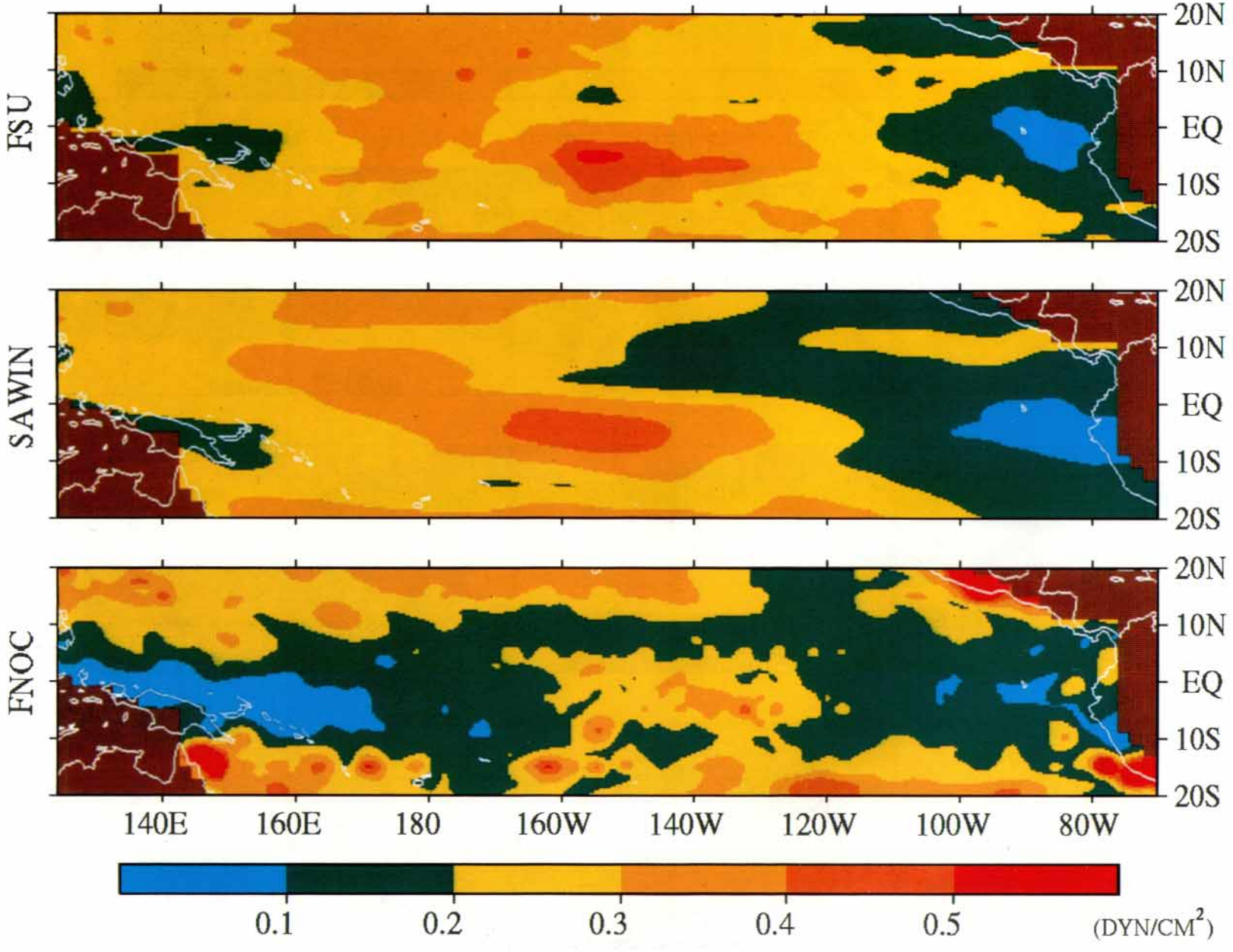

Fig. 13. Standard deviation of the interannual anomalies (1979–1983) about the mean seasonal cycle (1979–1981) of τ^x for: (Top) FSU (Middle) SAWIN (Bottom) FNOC

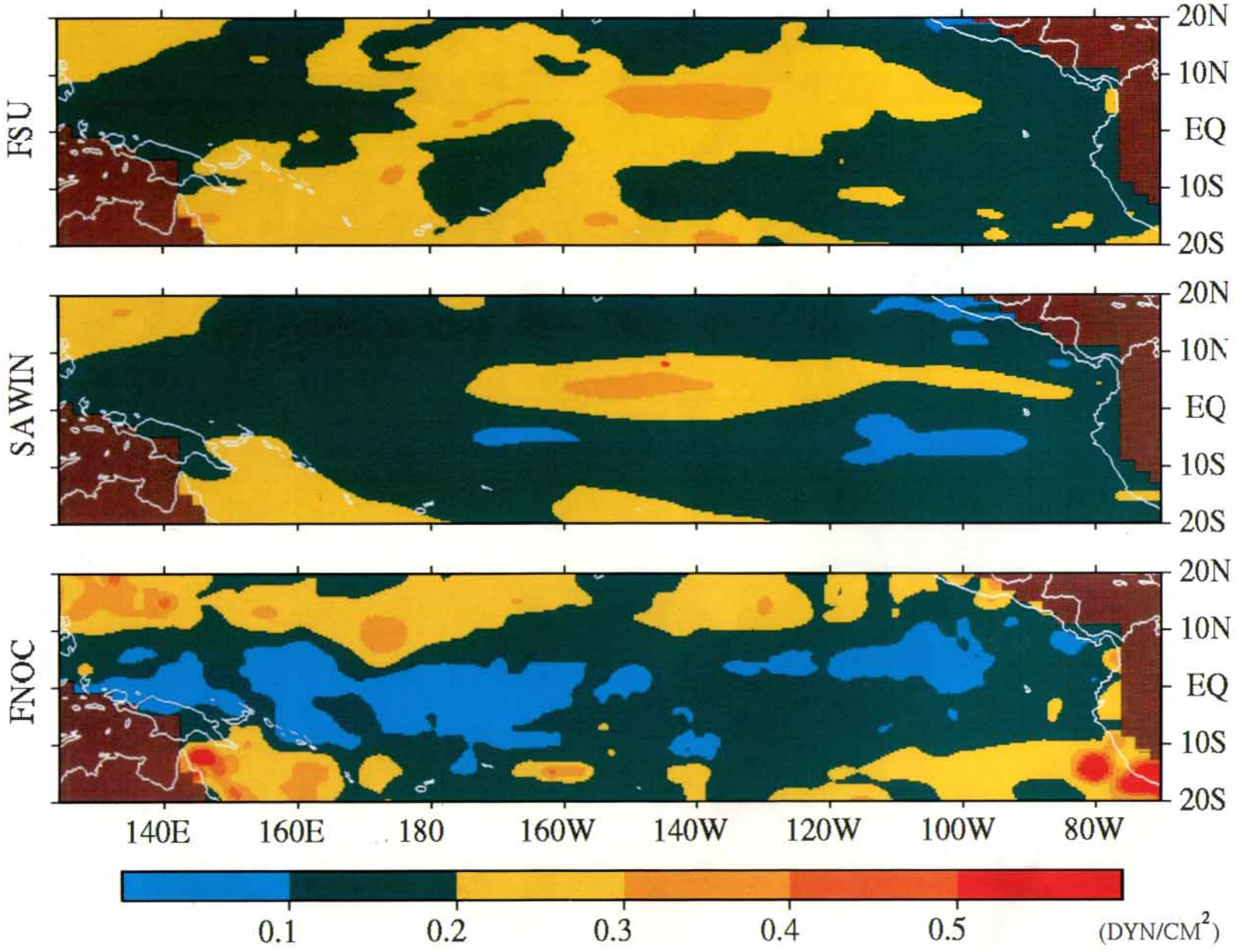

Fig. 14. Standard deviation of the interannual anomalies (1979–1983) about the mean seasonal cycle (1979–1981) of τ^y for: (Top) FSU (Middle) SAWIN (Bottom) FNOC

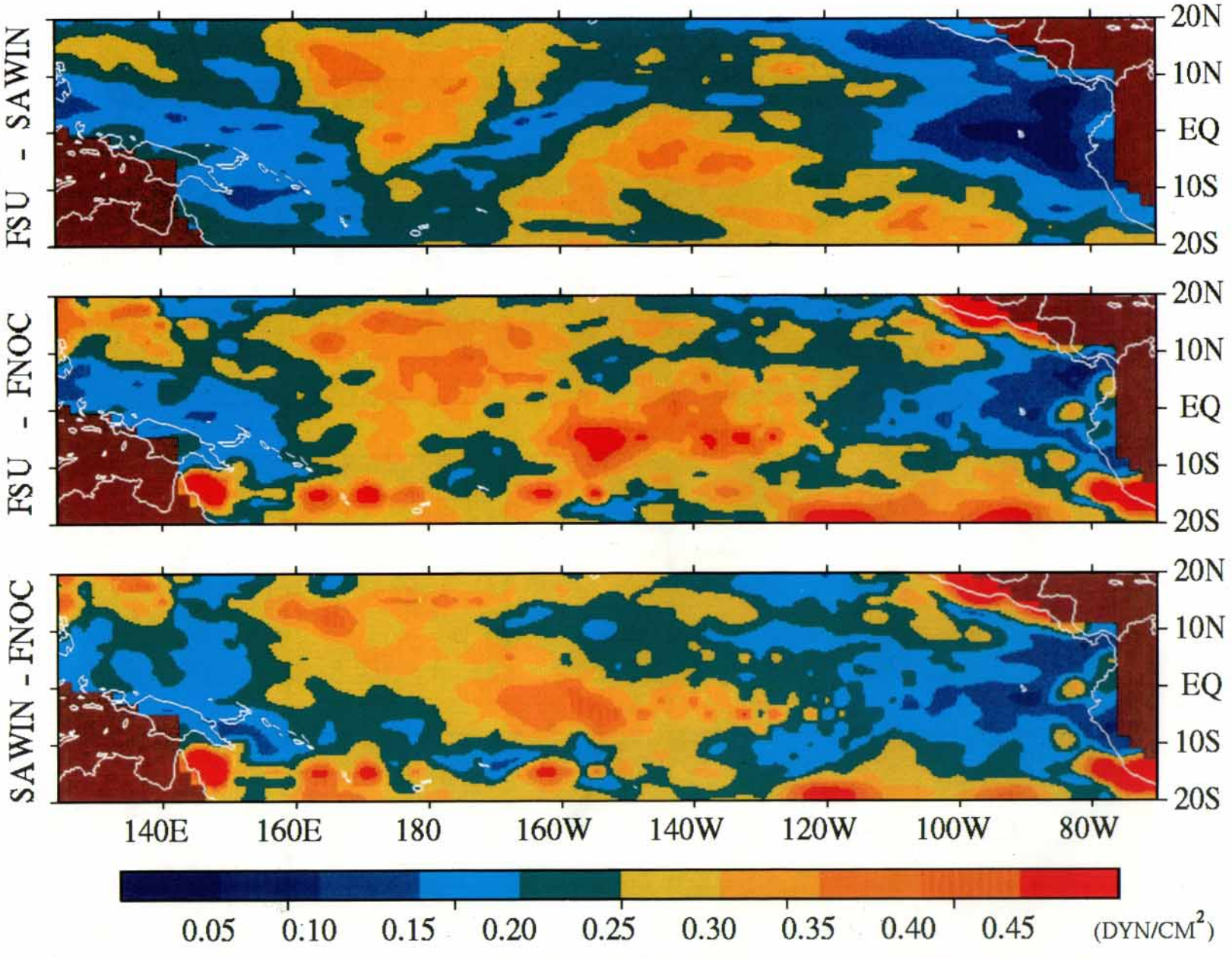

Fig. 15. Root mean square difference between the interannual anomalies (1979–1983) about the mean seasonal cycles of τ^x for: (Top) FSU-SAWIN (Middle) FSU-FNOC (Bottom) SAWIN-FNOC

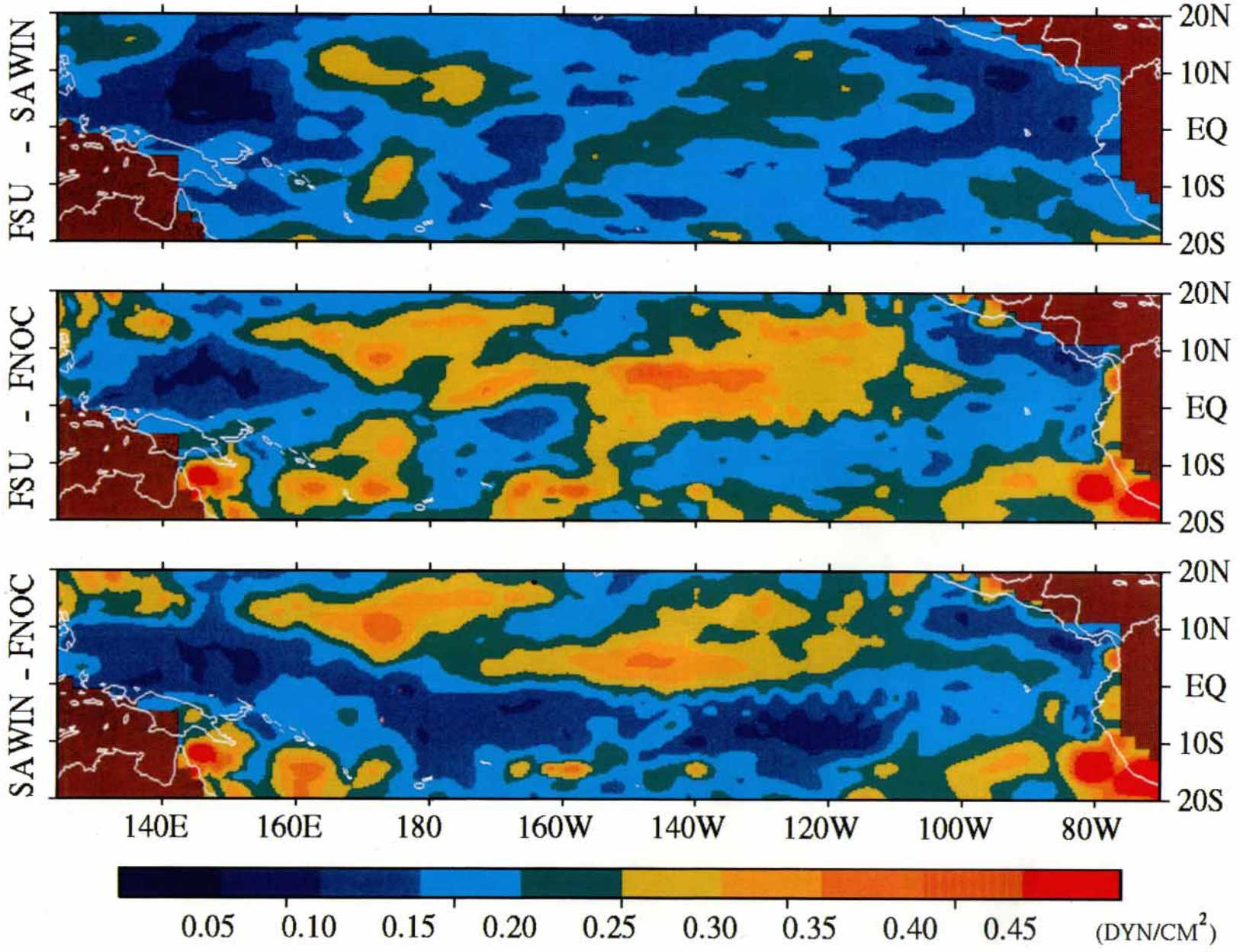

Fig. 16. Root mean square difference between the interannual anomalies (1979–1983) about the mean seasonal cycles of τ^y for: (Top) FSU-SAWIN (Middle) FSU-FNOC (Bottom) SAWIN-FNOC

are less than those obtained for the individual wind stress components.

(ii) Model sea level response

The seasonal model sea level response to forcing by the mean seasonal wind stress is summarized by Fig. 11. Common in the responses to all three wind products are maximum seasonal changes to sea level, $\sigma_s \sim 6$–10 cm, in the northeast quadrant of the basin. As reflected in the wind stress, the SAWIN-forced sea level solution exhibits larger maximum seasonal amplitudes and zonal length scales, most noticeably near the NECC, contrasted by little seasonal signal in the southeast. When averaged across the entire basin, the seasonal standard deviations for the FSU and SAWIN-forced sea levels are equivalent (see Table 1). Conversely, the FNOC-forced solution has the smallest seasonal response averaged across the basin. Consistent with the forcing, 60–80% of the variance for the mean seasonal sea level responses result from the annual harmonic.

Specific discrepancies in these sea level solutions are highlighted in the RMS difference fields (Fig. 12). Whereas the basin-scale wind stress components were similar, i.e. $\overline{\sigma_s}/\overline{\mathrm{RMSD}} > 1$, several important differences are apparent in the seasonal sea level variability, especially in the northern hemisphere. North of the equator, the maximum seasonal differences are in the vicinity of the NECC trough and the ITCZ. Note that these differences in the seasonal sea levels of order 6–10 cm are similar in magnitude to the maximum sea level signals (Fig. 11). The location of these significant sea level differences imply major differences in the variability and structure of the North Equatorial Current (NEC) and NECC in the three solutions. Other notable differences, ranging from 4 to 12 cm, are found beneath the SPCZ in the southwestern portion of the basin. The areally averaged $\overline{\mathrm{RMS}}$ differences are similar and range from 3.2 cm (FSU-SAWIN forced) to 3.6 cm (SAWIN-FNOC forced). When compared to the basin-wide mean seasonal standard deviations of sea level, signal-to-noise ratios of 0.9–1.2 are obtained, i.e., similar to those for the wind stress curl.

Interannual forcing and model sea level response

(a) Wind stress anomalies

The interannual variability is analyzed in terms of the anomalies for 1979–1983 about the mean seasonal cycle formed from the pre-El Niño years 1979–1981. The maximum interannual variations in τ^x are in the central Pacific (Fig. 13). The largest standard deviations of the τ^x anomalies, σ_i between 0.4 to 0.5 dyn cm^{-2}, are found near 150°W, 0° to 10°S in the FSU and SAWIN products. Inspection of the distributions for individual monthly anomalies indicates this interannual variability derives from anomalous westerly winds that extended into the central Pacific during the onset of the 1982–1983 El Niño. The maximum interannual variability in the FNOC zonal wind stress is smaller and further to the east. The interannual variability of τ^y is also similar in the FSU and SAWIN wind stress with $\sigma_i > 0.3$ dyn cm^{-2} near 4°N, 130°W–150°W (Fig. 14). There is no corresponding τ^y maximum in the FNOC data. Another aspect of the interannual variability of the FNOC wind stress components that is distinct from the FSU and SAWIN data is the greater degree of small spatial scale wind stress fluctuations near the coasts. The interannual variability of the wind stress curl formed from these components has no distinguishing features (not shown).

Similar to the interannual signal, some of the largest RMS differences in the interannual variability of the wind stress are in the central Pacific of order 0.25 to 0.5 dyn cm^{-2} (Figs. 15, 16). Regional differences with the FNOC wind stresses are greater than 0.5 dyn cm^{-2} near the coasts. The basin-wide mean $\overline{\mathrm{RMS}}$ differences of 0.23–0.27 dyn cm^{-2} for τ^x and 0.17–0.22 dyn cm^{-2} for τ^y are slightly greater than the basin-wide mean $\overline{\sigma_i}$ (Table 2) and imply signal-to-noise ratios of slightly less than 1.

One particularly noticeable aspect of the RMS differences is those regions of dense ship wind observations. Within the FSU-SAWIN RMS differences there is a clear indication of the influence of greater sampling along the central (Fiji–Hawaii) and western (Fiji–Japan) Pacific ship tracks. Along

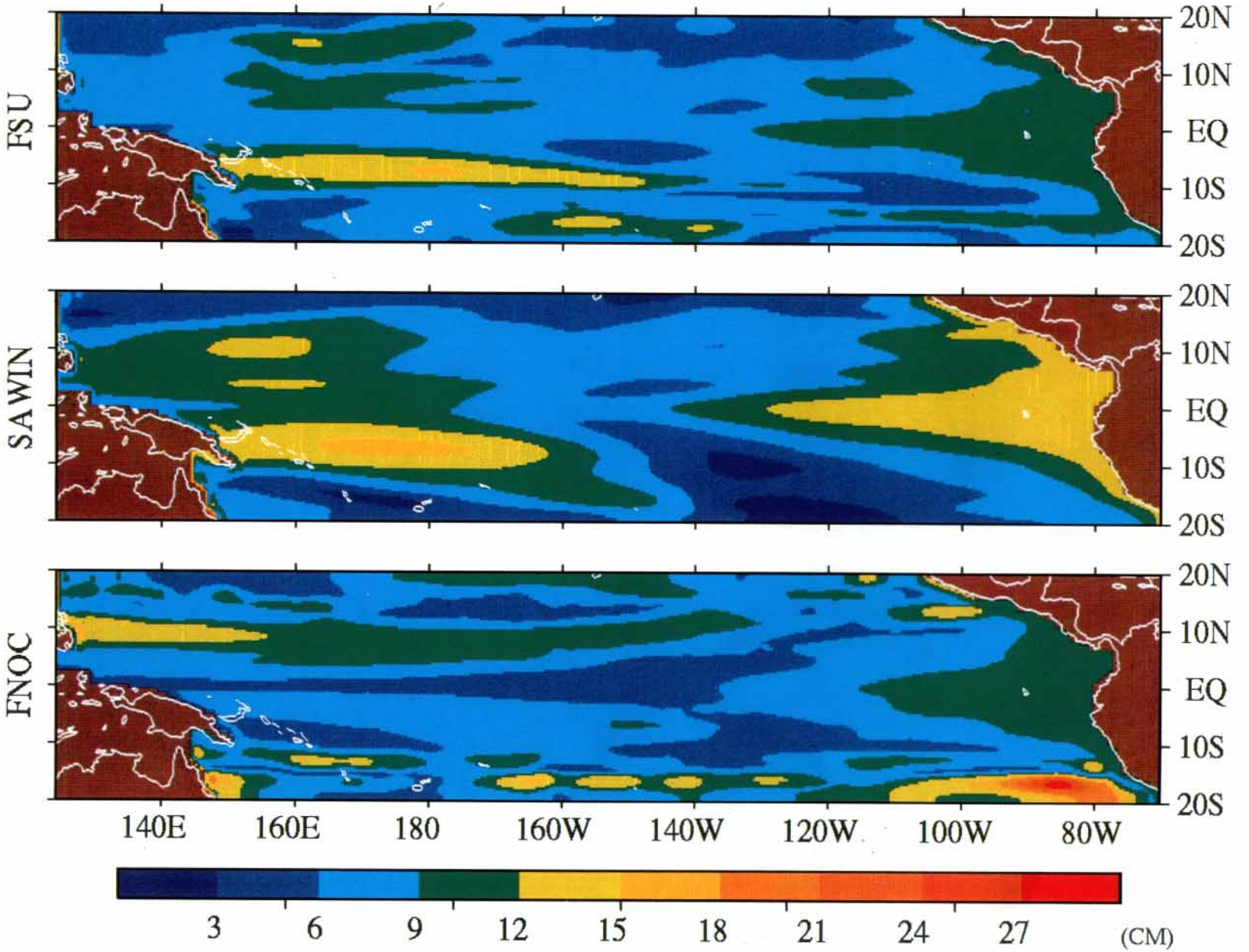

Fig. 17. Standard deviation of the interannual anomalies (1979–1983) about the mean seasonal cycle (1979–1981) of the model sea level in response to forcing by: (Top) FSU wind stress (Middle) SAWIN wind stress (Bottom) FNOC wind stress

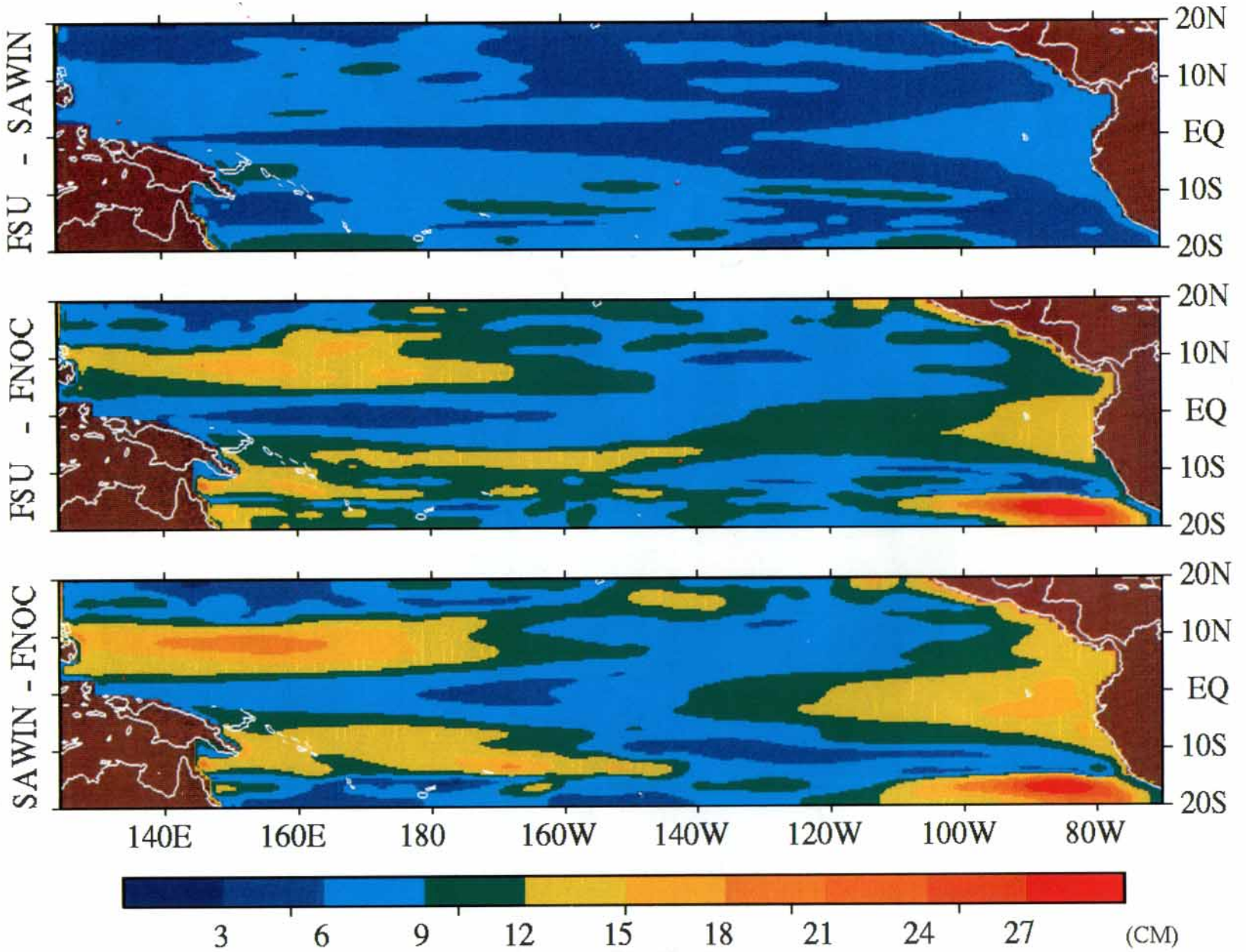

Fig. 18. Root mean square difference between the interannual anomalies (1979–1983) about the mean seasonal cycles of the model sea level in response to forcing by the two wind products: (Top) FSU-SAWIN (Middle) FSU-FNOC (Bottom) SAWIN-FNOC

these major shipping lines the RMS difference is often less than 0.2 dyn cm^{-2} and the signal/noise is greater than 1. In contrast, the largest RMS differences are located away from the ship tracks and for these areas the signal-to-noise ratio is considerably less than 1.

(b) Model sea level anomalies

Consistent with the presentation of the interannual wind stress variability, the interannual changes in the wind-driven model sea level are described in terms of the standard deviation of the

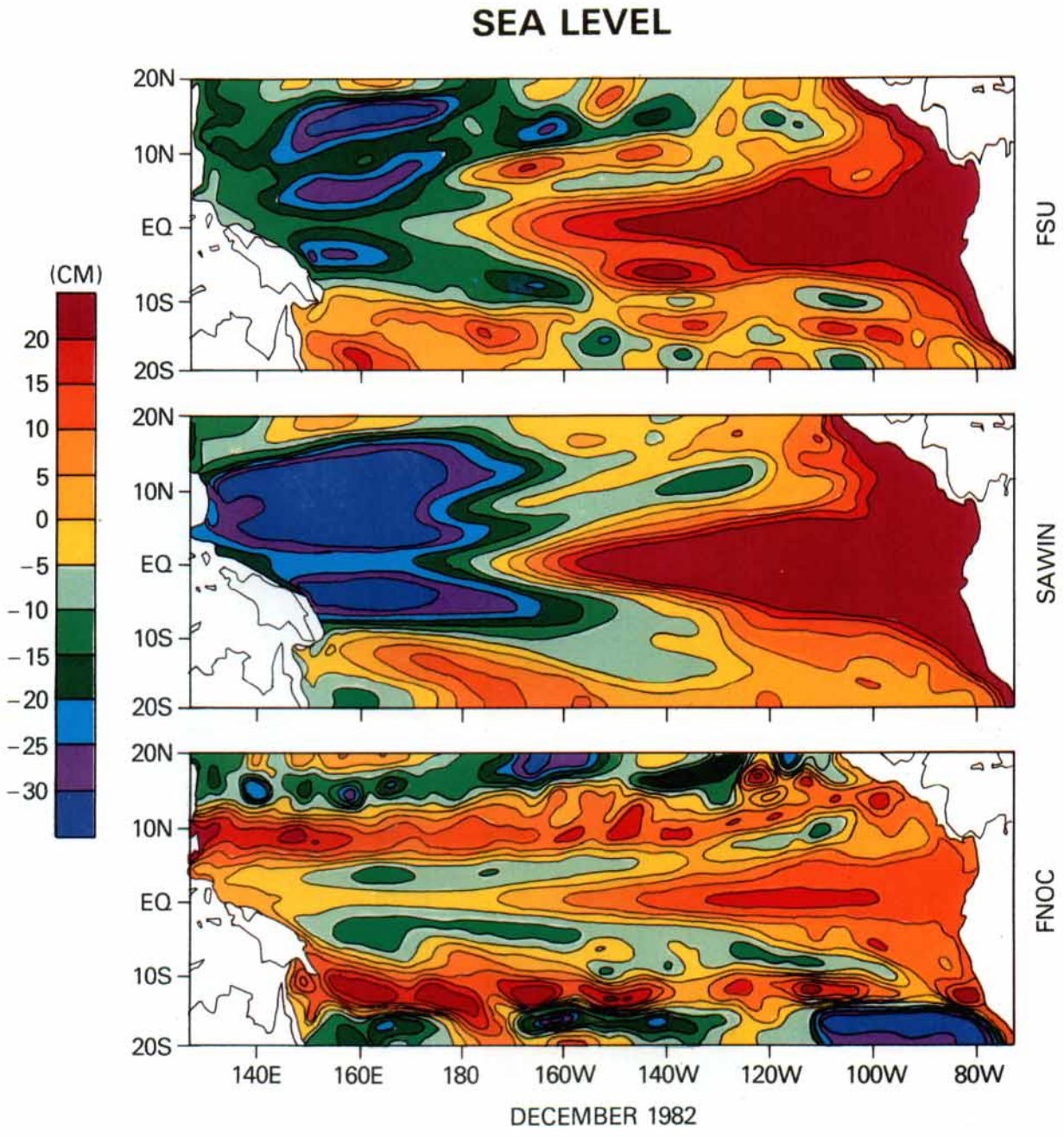

Fig. 19. Model sea level topography (less the annual mean) for December 1982 in response to forcing by: (Top) FSU wind stress (Middle) SAWIN wind stress (Bottom) FNOC wind stress

TABLE 2

Interannual anomalies 1979–1983

	τ^x (dyn cm^{-2})	τ^y (dyn cm^{-2})	$\nabla x \vec{\tau}$ (10^{-9} dyn cm^{-3})	sea level (cm)
Areally Averaged Standard Deviation ($\overline{\sigma_i}$)				
FSU	0.27	0.20	7.89	7.88
SAWIN	0.24	0.16	4.80	8.38
FNOC	0.21	0.17	7.04	8.04
Root Mean Square Difference ($\overline{\text{RMSD}}$)				
FSU-SAWIN	0.23	0.17	7.73	6.40
FSU-FNOC	0.27	0.22	10.30	9.74
SAWIN-FNOC	0.25	0.20	7.90	10.02

anomalies about the mean seasonal cycle (Fig. 17). Whereas the maximum seasonal sea level response was in the northeastern part of the basin, $\sigma_s \sim 6$–10 cm, the largest interannual variability, $\sigma_i \sim 12$–15 cm, is in the southwestern portion of the FSU and SAWIN-forced solutions. A second region of significant variation is the symmetric response about the equator in the east, $\sigma_i \sim 9$–12 cm. The largest contributions to the interannual signal for both of these regions are the 1982–1983 El Niño anomalies. Of the three solutions, the SAWIN-forced sea level is the most symmetric to the equator, and is suggestive of the signature of an equatorial Kelvin wave induced response in the east and an off equatorial Rossby wave induced response in the west. The SAWIN-forced sea level anomalies are also larger in amplitude and have larger spatial scales. The sea level solution in response to FNOC forcing is the most dissimilar. Both the FSU and FNOC forced solutions exhibit more small-scale structure south of 10°S.

Some of the qualitative differences alluded to above are quantified by the RMS differences of Fig. 18. The RMS differences between the sea level solutions forced by the two subjective analyses (FSU and SAWIN) are the smallest. The RMS difference for these solutions is at most 12 cm with a basin-wide mean of 6.4 cm (Table 2). In the mean these discrepancies are less than the interannual signal, $\overline{\sigma_i} \sim 7.9$–$8.4$ cm, but considerably more than the seasonal signal, $\overline{\sigma_s} \sim 3.1$–$3.8$ cm. The RMS differences involving the FNOC-forced sea level are significantly large with a basin-wide mean $\overline{\text{RMSD}} \sim 9.7$–$10.0$ cm and regional differences greater than 27 cm. When the FNOC differences are used to normalize $\overline{\sigma_i}$, the signal-to-noise is estimated to be well less than 1. In terms of the large-scale discrepancies between all of the sea level solutions, the largest differences are off the equator in the west, RSMD ~ 9–21 cm and on the equator in the east, RMSD ~ 6–18 cm. That is, the largest absolute error in the sea level solutions are found at the end of the appropriate equatorial wave characteristics.

Up until this point basin-wide statistics have been used to characterize the similarities and differences for the five years of wind products and sea level solutions. Although this is a convenient way to summarize the variability, it can also tend to obscure specific differences associated with individual events. In order to place the statistics of this section in the context of the 1982–1983 El Niño, we consider the mature phase of this event in December, 1982. Figure 19 clearly illustrates specific differences in the sea level evolution for the three simulations of this El Niño. The pattern of elevated sea level in the east is similar for the FSU and SAWIN-forced solutions and is consistent with a response to a relaxation or reversal of the equatorial easterlies. In the west, sea level is depressed to a greater extent north of the equator in response to the SAWIN wind stress and implies a greater redistribution of mass from west to east.

The scenario implied by the FSU and SAWIN-forced sea level distributions is not the case for the FNOC solution. In response to the FNOC wind stress, the El Niño event begins in the eastern 1/3 of the basin. The sea level response is also considerably smaller both in terms of the elevated sea level in the east and the depressed sea level in the west. Another significant difference is an anomalously high NECC trough across the entire basin. The implication of the NECC trough being filled in is a decrease to the eastward NECC and hence the redistribution of mass from west to east, both on the equator and off, is nowhere near as fully developed as in the FSU and SAWIN-forced solutions. The El Niño response depicted here is reflective of the σ_i of τ^x in Fig. 13 whereby the FNOC zonal wind stress anomalies were further

to the east and smaller than either the FSU or SAWIN wind stresses.

Model / Data intercomparison

In the previous section we discussed the similarities and differences between the FSU, SAWIN and FNOC wind products and how those affected model simulations for the period 1979–1983. We now turn our attention to a quantitative evaluation of these simulations by comparing them with oceanic observations for the same period. For this purpose we will use monthly mean estimates of (a) dynamic height relative to 400 db derived from ship-of-opportunity XBT data in the central Pacific and (b) island and coastal sea level data. Details about the processing of the XBT and sea level data can be found in Busalacchi and Cane (1985), McPhaden et al. (1988a, b), Picaut and Tournier (1990) and Springer et al. (1990).

(a) Comparison with central Pacific XBT dynamic heights

(i) Mean seasonal cycle

The results for the mean seasonal cycle are discussed at length by McPhaden et al. (1988a), but are summarized here for completeness. Figure 20 shows the standard deviation of surface dynamic height relative to 400 db from XBT data superimposed on the same calculation from the model simulations. The observed variability ranges between 1–7 dynamic cm, with maxima near 5° N and 12° N on either side of the mean position of the NECC trough. The FSU simulated variability is, in general, within 1–2 dynamic cm of the observations, except between the equator and 4° S where model variations are too large by 3–5 dynamic cm. SAWIN simulated variability is too large in this region also, whereas it tends to underestimate the magnitude of the fluctuations near the peak at 12° N. In the FNOC simulation, this peak is virtually absent, although the magnitude of simulated variability between 6° N and 6° S is more in agreement with observations than either in the FSU or SAWIN cases.

Extracting the 1 cycle per year harmonic which dominates the spectrum of variability in the observations and simulations, McPhaden et al. (1988a) found nearly in phase coherence of 0.5 between the modeled and observed dynamic heights between 20° N and 20° S. These coherences are significant at the 95% level of confidence, although they imply that only about 25% of the variance in the observed mean seasonal cycle can be explained by the model simulations in the central Pacific. Along the principal western Pacific

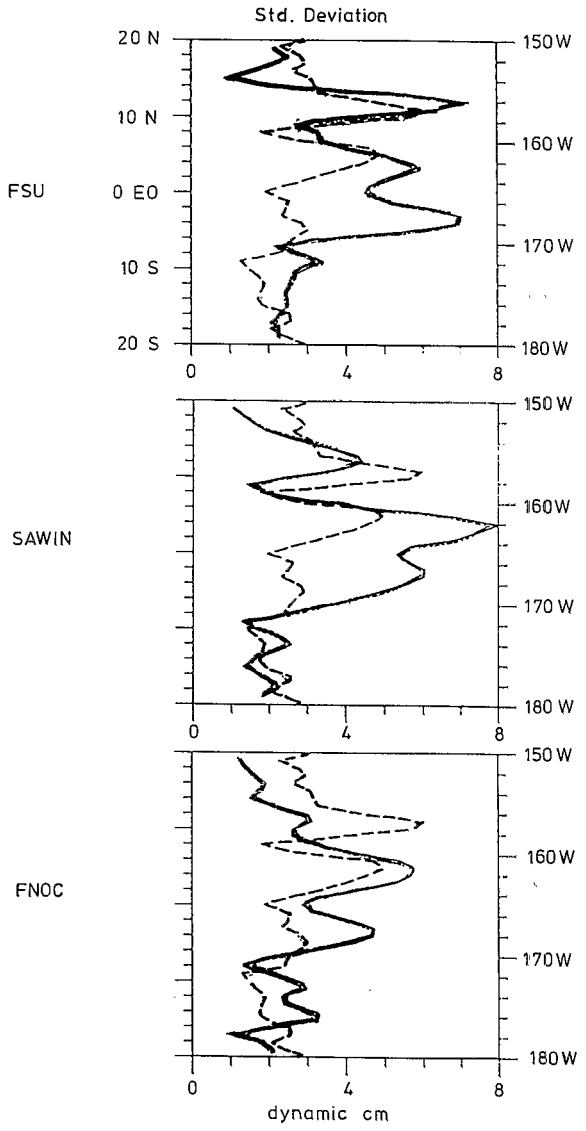

Fig. 20. Standard deviation of the mean seasonal cycle (1979–1981) of surface dynamic height relative to 400db along the central Pacific ship of opportunity track for XBT observations (dashed) and model simulations (solid) forced by: (Top) FSU wind stress (Middle) SAWIN wind stress (Bottom) FNOC wind stress

ship track annual coherence was as high as 0.7 between the FSU forced solution and the XBT-derived dynamic height and as low as 0.3 between the FNOC forced solution and the observations. Along an eastern Pacific track where annual amplitudes are smaller, the coherence estimates were only 0.3–0.5. The ensemble average coherence between the three model sea level solutions and time series from 29 tide gauge stations was 0.6.

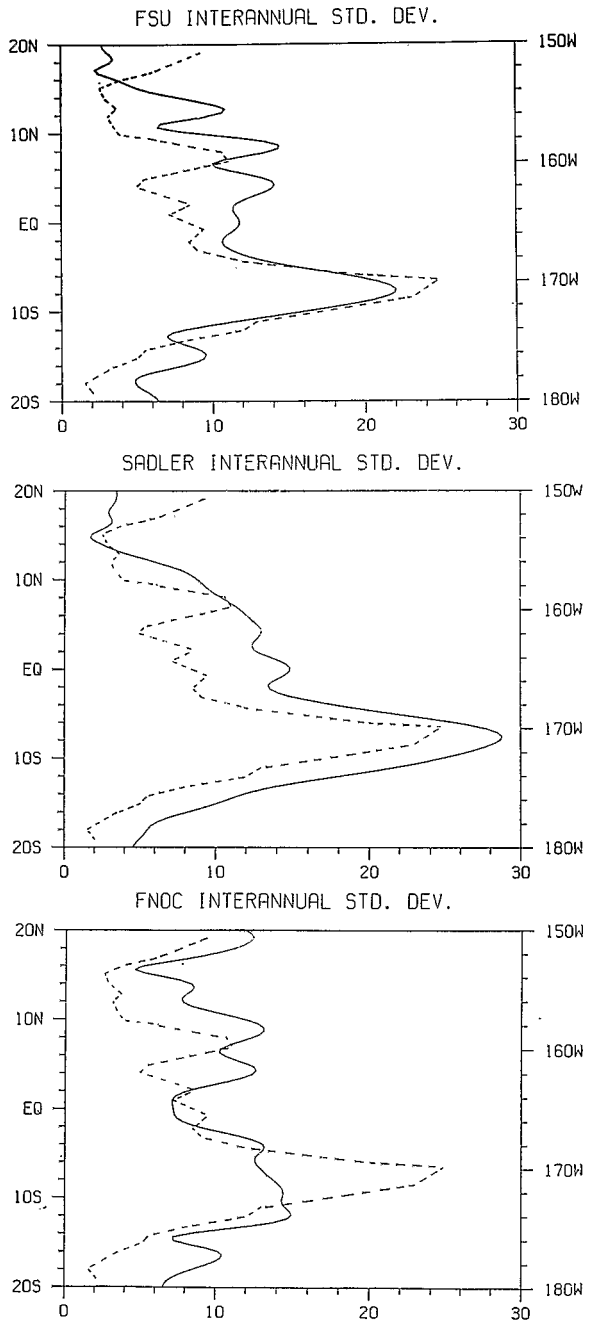

Fig. 21. Standard deviation of the anomalies for June 1982–July 1983 for observed dynamic height (dashed) and model sea level (solid) forced by: (Top) FSU wind stress (Middle) SAWIN wind stress (Bottom) FNOC wind stress

(ii) 1982–1983 anomalies

Figure 21 shows the standard deviation of observed dynamic height anomalies for June 1982–July 1983 superimposed on sea level anomalies for the same time period from the three model simulations. Simulated variability is presented in terms of sea level rather than dynamic height because the model output was not processed to dynamic heights for all three simulations. However, 1982–1983 FSU dynamic height anomalies shown in Fig. 5f of McPhaden et al. (1988b) and 1982–1983 FSU sea level anomalies shown here in Fig. 21 typically differ by < 2 cm. The observed variations are much larger than for the mean seasonal cycle, with magnitudes ranging between 6–24 dynamic cm in the central Pacific. The 24 dynamic cm peak near 8°S is due to a surface height depression in early 1983 which Kessler and Taft (1987) ascribe to anomalous Ekman pumping. The FSU and SAWIN forced simulations reproduce this peak near 8°S very well (with RMS sea level amplitudes of 22 cm and 29 cm, respectively). Conversely, FNOC simulated sea level variations are more hemispherically symmetric with a maximum amplitude of only 15 cm near 12°S. All three simulations tend to show more disagreement between 2°–12°N and between 2°–14°S. In some cases these differences are as large as 6 cm. None of the simulations produces a distinct singular peak at 7°–8°N as observed in the XBT data. As noted earlier this is an area, between the mean positions of the NECC ridge and trough, with some of the largest RMS differences among the model solutions.

(b) Comparison with sea level data

(i) Station comparisons

Figure 22 presents cross correlations between observed and simulated monthly mean sea level for the period 1979–1983 for 36 island and coastal sea level stations in the tropical Pacific. Similar analyses were presented in McPhaden et al. (1988a)

for the 1979–1981 mean seasonal cycle and in Busalacchi and Cane (1985) for the FSU wind-forced simulation during January 1982–March 1983. Results in the latter case are very similar to those presented here for the 5-year time period. Positive correlations between the observations and the FSU and SAWIN-forced simulations of > 0.7 (i.e. about 50% of the variance explained) can be found along the eastern boundary, along the equator and in the interior northwestern and southwestern Pacific. Correlations are generally smaller (and in some cases negative) along the western boundary and near the open boundaries at 20° N and 20° S. The correlation of the sea level ob-

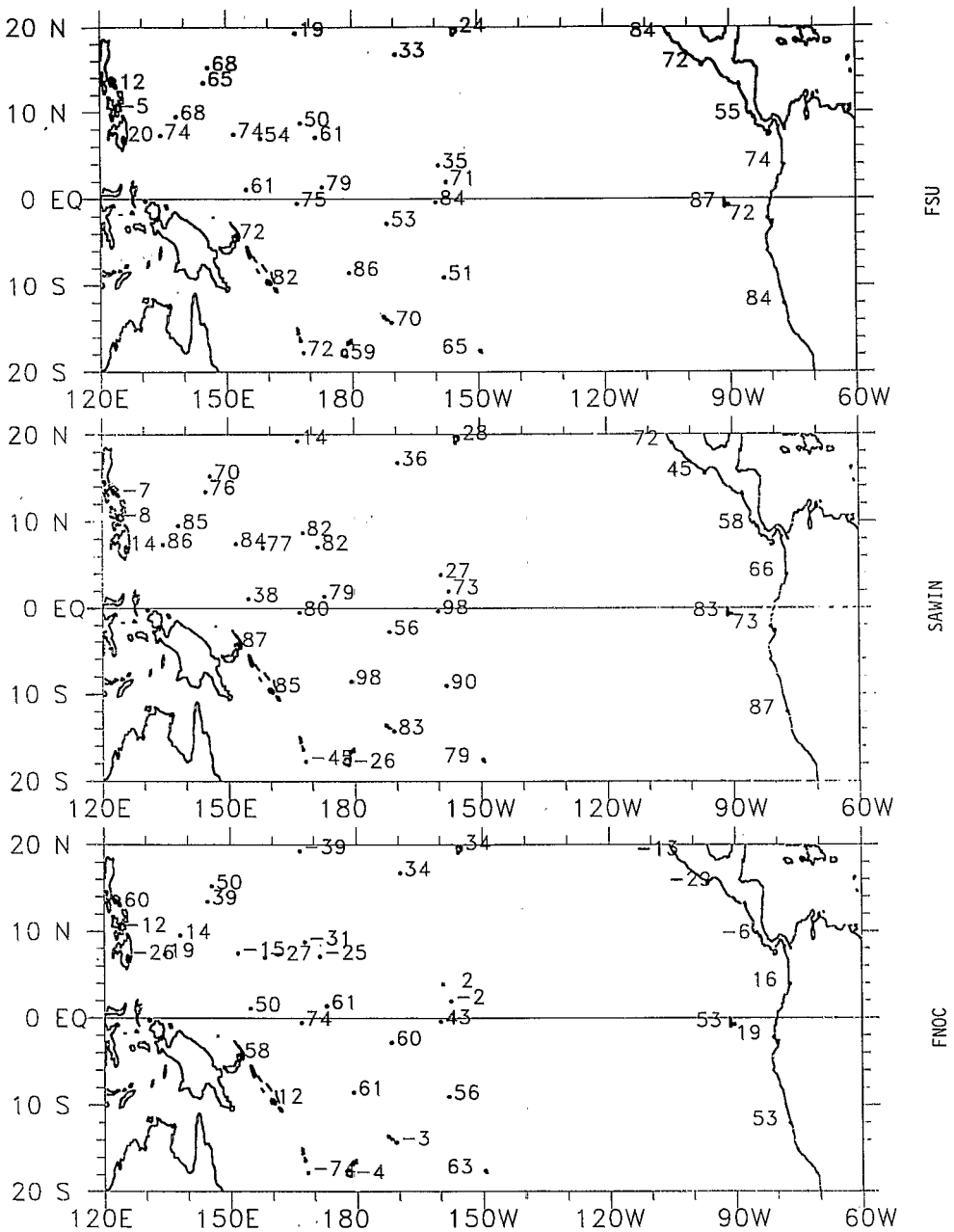

Fig. 22. Cross correlations between monthly mean sea level observations, 1979–1983, and the model sea level simulations forced by: (Top) FSU wind stress (Middle) SAWIN wind stress (Bottom) FNOC wind stress

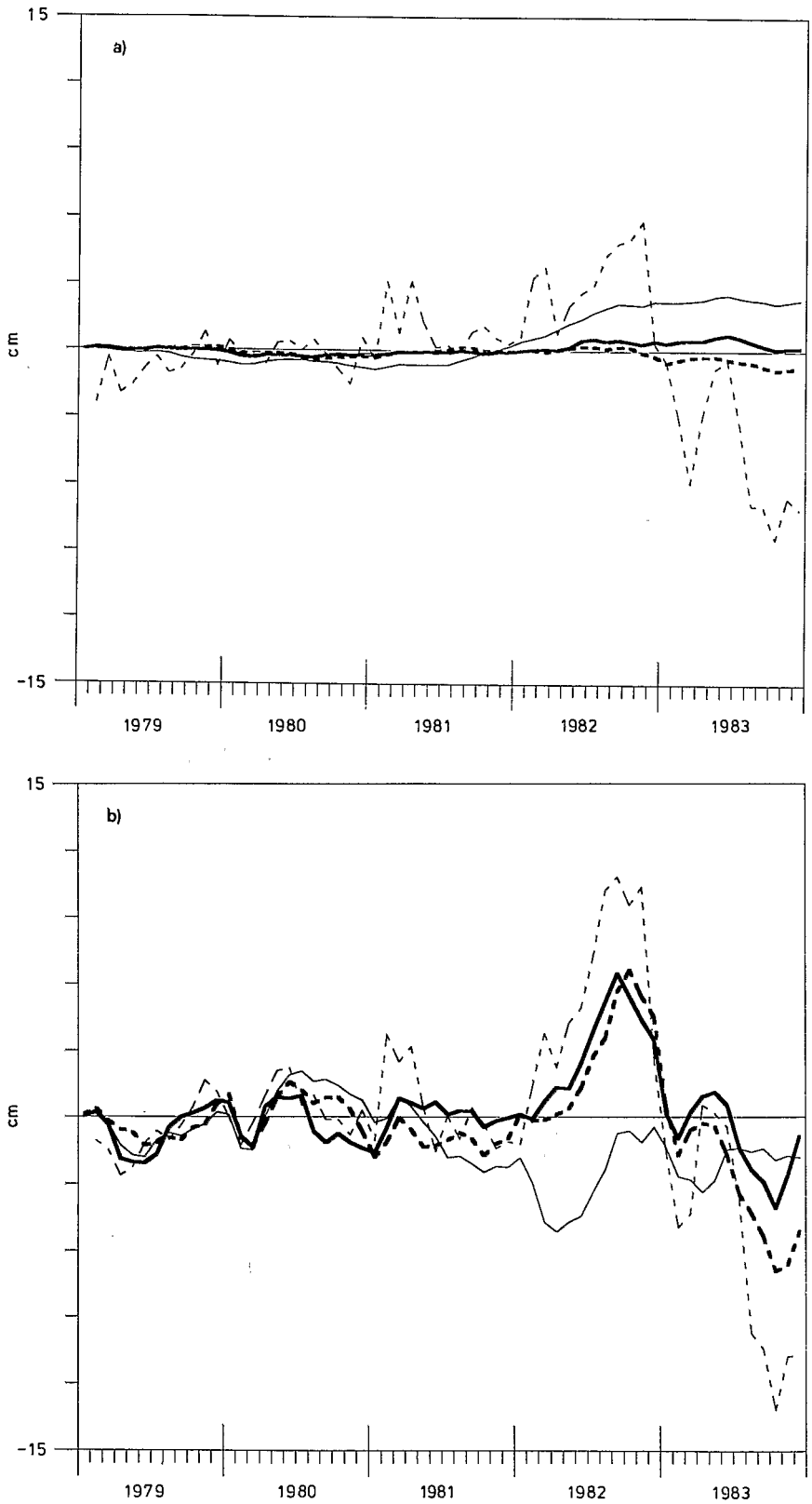

Fig. 23. Areally averaged sea level anomalies, 1979–1983, for the three wind-forced sea level solutions (FSU-heavy, SAWIN-heavy dashed, FNOC-thin) and gridded tide gauge observations (thin dashed): a) 15°N–15°S b) 5°N–5°S

servations with the FNOC wind forced simulation is, in contrast, generally much lower than in the case of the FSU and SAWIN simulations. Indeed, several negative FNOC sea level correlations are found in the vicinity of 8° N in the western Pacific. There the observations showed a deepening of the NECC trough while the FNOC simulation indicated an elevation of the trough during 1982–1983. Recall that Fig. 19 shows this anomalous elevation of the NECC trough all the way across the basin in the FNOC simulation. The average of all the correlation coefficients in Fig. 22 is 0.60 (FSU), 0.58 (SAWIN) and 0.17 (FNOC); this clearly identifies the FNOC calculation as having the least hindcast skill for sea level.

(ii) Areal averaged sea level

Figures 23a and 23b show areally averaged model sea level anomaly plots for latitude bands 15° N–15° S and 5° N–5° S, respectively. Overplotted on these are areally averaged sea level anomalies from the island and coastal stations. We gridded the observed sea level station data as in Wyrtki (1985), who converted his analyzed field to an equivalent upper layer volume assuming that the ocean behaves as a 2-layer system. We do not make this assumption in the following discussion in order to permit more direct comparison with the simulated sea levels. However, the analysis shown in Fig. 23a is essentially that presented in Wyrtki (1985) except for a constant of proportionality relating sea level to upper ocean volume.

Figure 23a indicates that in the FSU and SAWIN simulations, there is effectively no net change in sea level between 15° N–15° S over the 5 year period. This differs markedly from the FNOC case in which there is a significant elevation during 1982 and 1983 due to the (erroneously) elevated sea level in the NECC trough as noted earlier. However, none of these simulations compares favorably with the observational analysis. Springer et al. (1990) note that this is due to the spatial resolution of the sea level network which in the eastern Pacific aliases the dominant zonal length scales. The result is an observational analysis which inaccurately reflects averaged sea level changes in the latitude band 15° N–15° S.

Figure 23b shows a much better comparison between the FSU, SAWIN and analyzed observations between 5° N–5° S. The principal reason for this is that the zonal length scales of sea level are longer near the equator and hence are reasonably well resolved by the spacing of the tide gauge network. The timing of the peaks and troughs in both simulations is well represented in 1982 and 1983; the magnitude of the FSU and SAWIN simulated peaks in late 1982 are very close to that observed, though the sea level minima in 1983 tend to be underestimated (especially for the FSU case). Neither the FSU nor the SAWIN simulation fully captures the onset of the event in early 1982 or the smaller amplitude non-ENSO interannual anomalies during 1979–1981. Conversely, the FNOC simulation misses even the large 1982–1983 ENSO anomalies, consistent with the poor station by station correlations shown in Fig. 22.

The relatively successful FSU and SAWIN hindcasts of 1982–1983 ENSO sea level anomalies suggests that most of the 5° N–5° S changes in sea level (or equivalently upper ocean volume) were compensated for by changes between 5°–15°. Springer et al. (1990) elaborate on the oceanic processes involved in this compensation in the FSU simulation. These results are consistent with the coupled ocean model results of Zebiak and Cane (1987) who identified 5° N–5° S as the band of latitudes where the most relevant average changes in upper ocean volume occur on ENSO time scales.

Summary and conclusions

The previous sections served to reveal the similarities and differences in several wind stress data sets representative of the type and quality presently available for use as forcing functions in multiyear tropical ocean simulations. The signal and discrepancies in the zonal wind stress, the meridional wind stress, and the wind stress curl were quantified on time scales ranging from the mean seasonal cycle to those for an extreme El Niño event. The sensitivity of the seasonal and interannual wind-driven response to such forcing was assessed using a linear ocean model as a transfer function for the wind data. The effect of uncertainties in the seasonal and interannual wind

forcing was illustrated by intercomparison between the model sea level simulations and subsequent comparison with in situ sea level data. The results of these analyses have revealed important qualitative and quantitative differences in various wind products and the resultant impact on wind-driven ocean simulations.

At the time of this study there were only three possible tropical Pacific wind products in which the wind analysis schemes were held constant over a period of years that included both a typical seasonal cycle and also an El Niño occurrence. The two subjective analyses of FSU and SAWIN and the one operational objective analysis from FNOC were considered for the five years 1979–1983. Overall, the two subjective analyses were the most similar of the three wind products.

The large-scale mean features of the northeast and southeast trade wind systems were common to all three data sets. One particular exception was a more southern position of the ITCZ in the FNOC data. Formation of the wind stress curl proved to be an effective discriminator of the wind fields. Differencing the wind stress components tended to amplify the small-scale structure present in the FNOC data and to a lesser extent in the FSU data. The most fundamental differences in the mean wind stress fields was a continuous band of negative wind stress curl in the southern hemisphere of the FNOC data that had no counterpart in the FSU or SAWIN data.

Seasonal variability of the zonal and meridional wind stress was very similar in the FSU and SAWIN data. Weaker seasonal changes to the northeast trades in the FNOC data set this product apart from the others. Some of the largest regional differences in the seasonal variability of the wind products, differences greater than 0.2 dyn cm^{-2}, corresponded to the ITCZ in the northern hemisphere and the SPCZ in the southern hemisphere. In all three products the basin-scale seasonal variability of the wind stress components was very robust compared to the discrepancies among the products; mean seasonal standard deviations of order 0.16–0.25 dyn cm^{-2} compared to mean root mean square differences between the wind sets of order 0.09–0.17 dyn cm^{-2}. This was not the case, however, when the seasonal variability was considered in terms of the wind stress curl, which is the most appropriate representation of the wind stress when considering the off-equatorial oceanic response. As in the mean wind stress curl distribution, small-scale structure was magnified in the FNOC seasonal wind stress curl and to a lesser degree in the FSU data. Unique to the SAWIN data was a broad region of little seasonal change to wind stress curl in the southeastern quadrant of the basin. In contrast to the wind stress components, the seasonal signal of the wind stress curl (represented by the mean standard deviations) was roughly the same order as the noise or uncertainty in the seasonal changes to the wind stress curl (represented by the mean root mean square differences).

Interannual anomalies about the mean seasonal cycle were similar in the FSU and SAWIN winds and were dominated by the relaxation of the equatorial easterlies in the central Pacific during the 1982–1983 El Niño. The anomalies in the FNOC data were smaller and to the east. Unlike the seasonal variability, the interannual anomalies of the wind stress components were not large relative to the difference between the product anomalies. The mean standard deviation of the anomalies about the seasonal cycle were 0.16–0.27 dyn cm^{-2} while the mean root mean square differences of the anomalies were of similar magnitude of 0.17–0.27 dyn cm^{-2}. The dependence on ship wind observations was apparent along the major ship tracks in the central and western Pacific where the discrepancies in the wind stress anomalies were as small as 0.1 to 0.2 dyn cm^{-2}. Away from the major shipping lanes RMS differences in the anomalies reached up to 0.5 dyn cm^{-2}. The differences among the wind products increased even more relative to the signal of the anomalies when the wind stress curl was formed.

The implications of these similarities and differences in the wind fields with respect to the forced integrated oceanic response were assessed using the sea level solutions from a linear, multimode numerical model. The efficiency of this linear approach made it possible to consider several different multiyear wind products. Being able to consider three different wind products of five years in length allowed us to investigate the effects of

limitations to the wind data on both seasonal and interannual time scales.

In response to the mean annual forcing, the sea level topography was similar for all three model solutions, but for one important exception. As a result of the continuous band of negative mean wind stress curl for the FNOC data in the southern hemisphere, a mean SECC trough was formed that had no counterpart in the other solutions. Small-scale structure apparent in the mean wind stress components and wind stress curl fields was not reflected in the mean sea level topographies.

The largest sea level response to the seasonal wind forcing was in the northeastern and central portion of the basin as evidenced by standard deviations of order 6–10 cm. Uncertainties in the seasonal wind fields, primarily those associated with the description of the wind stress curl near the ITCZ, were manifested in the model sea level solutions as 6–12 cm RMS discrepancies in the vicinity of the NECC trough. Significant differences in the three solutions were also found to correspond with another important atmospheric convergence zone, namely the SPCZ in the southern hemisphere. In terms of basin-wide averages, the mean seasonal standard deviations of sea level for the three solutions, 3.1–3.8 cm, were of similar magnitude to the discrepancies among the three sea level solutions, 3.2–3.6 cm. The approximate signal-to-noise estimates that are inferred by these measures are more in keeping with those for the wind stress curl than any conclusions that would be drawn by considering only the wind stress components. The implications of a weak seasonal signal relative to the uncertainties was also borne out by annual coherence estimates between the model sea levels and observational data (XBT-derived dynamic heights and tide gauge sea levels) that ranged from 0.3 to 0.7.

The interannual variability of the model sea level was dominated by the anomalies associated with the 1982–1983 El Niño. The interannual signal was most similar between the FSU and SAWIN-forced sea level solutions; mean $\overline{\text{RMS}}$ difference of 6.4 cm compared to standard deviations of the mean sea level anomalies of 7.9 cm (FSU) and 8.4 cm (SAWIN). Considerably larger mean $\overline{\text{RMS}}$ differences, 9.7–10 cm, were obtained with the FNOC-forced sea levels because the El Niño was not as fully developed. Point differences with the FNOC solution were greater than 20 cm in certain locations. To place these errors in context, observed sea level changes typical of a weak or moderate El Niño are also of order 20 cm.

Cross correlations with observed sea level were consistent with the signal-to-noise ratios that imply a signal greater than the uncertainties when considering the FSU or SAWIN-forced interannual solutions, but a signal less than the uncertainty when involving the FNOC forcing. Cross correlations between the FSU-forced solutions and observed sea level at 36 island and coastal stations ranged between -0.05 to 0.87 with an ensemble averaged correlation of 0.60. Correlations between the SAWIN-forced sea level solutions with the observed sea level ranged between -0.45 to 0.98 and had an ensemble mean correlation of 0.58. The skill of the hindcast driven by the FNOC winds was significantly less. Correlation coefficients ranged between -0.74 to 0.74 with an ensemble mean of 0.17. Model versus model correlations also depicted the FNOC forced solution as the lone outlier. The ensemble mean correlations between the model sea level solutions were FSU versus SAWIN $r = 0.69$, FSU versus FNOC $r = 0.33$ and FNOC versus SAWIN $r = 0.36$.

The results of this study have revealed several problems in the observations and description of the surface wind field and resultant forced oceanic response for the tropical Pacific. With respect to the wind field, recall that the TOGA Program accuracy requirement for monthly mean surface wind stress was 0.1 dyn cm^{-2} over spatial scales of 2° latitude $\times$10° longitude. The $\overline{\text{RMS}}$ differences between the mean seasonal wind products were approximately 1.5 times greater than this requirements, whereas the $\overline{\text{RMS}}$ difference in the interannual anomalies was 2.5 times greater. Although these estimates of uncertainties in the wind stress components may compare favorably relative to the amplitudes of the seasonal and interannual signals, they yield little information, if any, as to how well gradients in the wind field are being described. In view of the fact that some of the most critical differences in the wind stress products were in wind regimes of surface convergence

and significant gradients such as the ITCZ and SPCZ, special emphasis needs to be placed on the wind stress curl fields when evaluating wind products for use in oceanographic applications. Moreover, consideration of the wind stress curl variability should encompass both the seasonal and interannual variability. One of the reasons why the subjectively analyzed FSU and SAWIN products were superior to the objectively analyzed FNOC wind data is the structure and variability of the wind stress curl fields. Since the subjectively analyzed products were intended for research applications, the location and structure of features such as convergence zones and the wind stress curl fields were taken into consideration as part of the analyses. Significant improvements in resolving gradients in the wind stress, most importantly $\partial\tau^x/\partial y$, are not likely until more dense spatial sampling is provided by such techniques as satellite scatterometry. The assimilation into an atmospheric general circulation model of surface wind speeds estimated from satellite microwave measurements (Atlas and Bloom, 1989), albeit a scalar measure, shows some promise as an interim improvement until scatterometer retrievals from ERS-1 and NSCAT are available and rigorously validated.

Our use of a five-year time series pointed to another problem in using operational center analyses. Only the FSU, SAWIN and FNOC wind stress data sets were considered to be permissible for our study of the seasonal and interannual variability, as these were the only products available for which there was a consistent analysis scheme in place for the entire five years. Periodic improvements and changes to the analysis schemes at other operational centers such as ECMWF and NMC precluded the use of these products (Bengsston and Shukla, 1989). A consistent analysis scheme is essential to any research investigation of interannual variability. The importance of the El Niño phenomenon brings this issue to the forefront. The problems encountered here clearly demonstrate the need, sometime during the TOGA decade, for a reanalysis of atmospheric model based data such that a multiyear record of surface winds is produced with an internally consistent analysis. The subsequent use and scrutiny of these winds in ocean simulation studies should prove very helpful in evaluating the reanalyzed atmospheric data.

In terms of the wind-forced oceanic response, increased attention is in order for those regions subject to the largest wind stress curl variations. Some of the largest uncertainties in the model sea level solutions were in the vicinity of the NECC trough; a feature that is subject to large changes in the wind stress curl caused by annual and interannual excursions of the ITCZ. The same arguments also apply to the sea level response beneath the SPCZ in the southern hemisphere. Previously, McPhaden et al. (1988a) noted that the largest simulated seasonal sea level response occurs in the northeastern tropical Pacific in the region that is not routinely sampled by XBT, tide gauge, or current meter measurements. In view of the large-amplitude forcing in such areas, the NECC variability should be a routine critical test of any tropical Pacific model simulation. The verification of such a potentially important signal will be impossible without additional in situ measurements in the region.

Related efforts with these model sea level solutions have shown that the location and spacing of tide gauge measurements within $\pm 5°$ of the equator are capable of providing very useful estimates of changes in upper ocean volume within this latitudinal band. When the latitudinal band in question is extended poleward, the zonal spacing between island stations becomes large relative to the zonal decorrelation scales of sea level variability. That is, outside the equatorial wave guide, the tide gauge station spacing may not be suitable for making volume estimates over large regions. The sea level simulations presented here suggested that subsampling errors introduced when estimating changes to upper ocean volume with island sea level measurements within $\pm 15°$ are larger than the errors introduced into such estimates by differences in the various wind fields used as forcing functions. As with the coverage problems encountered in describing the surface wind field, accurate depictions of the large-scale variability of sea surface topography in the tropics may not be possible until satellite altimeter measurements such as those from GEOSAT and TOPEX/POSEI-

DON are rigorously validated and analyzed in concert with available in situ measurements.

Acknowledgements

The authors would like to thank J.J. O'Brien for providing the FSU wind product, J. Sadler for providing the SAWIN wind product and J.C. Kindle for providing the FNOC wind product used in this study. This work was supported by NASA research task operating plan 161-20-31 and Jet Propulsion Laboratory contract 957647 (AJB), NOAA's Equatorial Pacific Ocean Climate Studies (EPOCS) program (MJM), the Institut Français de Recherche Scientifique pour le Développement en Coopération (JP) and the School of Oceanography, University of Washington (SRS). The assistance provided by J. Beauchamp and J. Braatz III is greatly appreciated. NOAA PMEL contribution 1170 and JISAO contribution 66.

References

Atlas, R. and Bloom, S., 1989. Global surface wind vectors resulting from the assimilation of satellite wind speed data in atmospheric general circulation models. Oceans '89 Proceedings, September 18–21, 1989, Seattle, WA. IEEE Publ., 89CH2780-5: 260–265.

Bengtsson, L., and Shukla, J., 1988. Integration of space and in situ observations to study global climate change. Bull. Am. Meteorol. Soc., 69: 1130–1143.

Busalacchi, A.J. and Cane, M.A., 1985. Hindcasts of sea level variations during the 1982–83 El Niño. J. Phys. Oceanogr., 15: 213–221.

Cressman, G.P., 1959. An operational objective analysis system. Mon. Weather Rev., 87: 367–374.

Enfield, D., 1989. El Niño, past and present. Rev. Geophys., 27-2: 159–187.

Eriksen, C.C., Blumenthal, M.B., Hayes, S.P. and Ripa, P., 1983. Wind-generated equatorial Kelvin waves observed across the Pacific Ocean. J. Phys. Oceanogr., 13: 1622–1640.

Goldenberg, S.B. and O'Brien, J.J., 1981. Time and space variability of tropical Pacific wind stress. Mon. Weather Rev., 109: 1190–1207.

Harrison, D.E., Kessler, W.S. and Geise, B.S., 1989. Ocean circulation model hindcasts of the 1982-83 El Niño: Thermal variability along the ship-of-opportunity tracks. J. Phys. Oceanogr., 19: 397–418.

Hayes, S.P., 1989. The Atlas wind and thermal structure array. In: "US TOGA Ocean Observation System Mid-life Progress Review and Recommendations for Continuation." Workshop rep., Kaimana Beach Hotel, Honolulu, HI, March 8–10, 1989. Nova Univ. Press, Ft. Lauderdale, FL.

Kessler, W.S. and Taft, B.A., 1987. Dynamic heights and zonal geostrophic transports in the central tropical Pacific during 1979–84. J. Phys. Oceanogr., 17: 97–122.

Landsteiner, M.C., McPhaden, M.J. and Picaut, J., 1990. On the sensitivity of Sverdrup transport estimates to the specification of wind stress forcing in the tropical Pacific. J. Geophys. Res., in press.

McPhaden, M.J., Busalacchi, A.J. and Picaut, J., 1988a. Observations and wind-forced model simulations of the mean seasonal cycle in tropical Pacific sea surface topography. J. Geophys. Res., 93: 8131–8146.

McPhaden, M.J., Busalacchi, A.J., Picaut, J. and Raymond, G., 1988b. A model study of potential sampling errors due to data scatter around expendable bathythermograph transects in the tropical Pacific. J. Geophys. Res., 93: 8119–8130.

Picaut, J. and Tournier, R., 1990. Monitoring the 1979–85 equatorial Pacific current transport with XBT data. J. Geophys. Res., (submitted).

Roed, L.P. and Smedstad, O.M., 1984. Open boundary conditions for forced waves in a rotating fluid. SIAM J. Sci. Stat. Comput., 5: 414–426.

Sadler, J.C. and Kilonsky, B.J., 1985. Deriving surface winds from satellite observations of low-level cloud motions. J. Clim. Appl. Meteorol., 24: 758–769.

Sadler, J.C., Lander, M.A., Hori, A.M. and Oda, L.K., 1987. Tropical marine climatic atlas, II, Pacific Ocean, Techn. Rep. UHMET 87-02, Dep. Meteorol., Univ. Hawaii, Honolulu.

Springer, S.R., McPhaden, M.J. and Busalacchi, A.J., 1990. Oceanic heat content variability in the tropical Pacific during the 1982–1983 El Niño. J. Geophys. Res., (submitted).

World Climate Research Program, 1971, Scientific Plan for the Tropical Ocean and Global Atmosphere Programme. WCRP Publ. Ser. 3, 146 pp.

Wyrtki, K., 1985. Water displacements in the Pacific and the genesis of El Niño cycles. J. Geophys. Res., 90: 7129–7132.

Zebiak, S.E. and Cane, M.A., 1987. A model El Niño/Southern Oscillation. Mon. Weather Rev., 115: 2262–2278.